NASA Contractor Report 165939

Active Flutter Suppression Using Optimal Output Feedback Digital Controllers

J. R. Broussard and N. Halyo

INFORMATION & CONTROL SYSTEMS, INCORPORATED
Hampton, VA 23666

Contract NAS1-16772
May 1982

NASA
National Aeronautics and
Space Administration

Langley Research Center
Hampton, Virginia 23665

FOREWORD

The investigation described in this report was performed by Information & Control Systems, Incorporated (ICS) during the period from October 1981 to March 1982, under Contract Number NAS1-16772 for the National Aeronautics and Space Administration, Langley Research Center, Hampton, Virginia. This work was sponsored by the Flight Controls Systems Division. Mr. Aaron J. Ostroff served as Technical Representative monitoring this contract. Dr. Nesim Halyo was the ICS Program Manager. Mr. John R. Broussard was the Principal Investigator. Programming support at ICS was provided by Richard W. Samms and Deborah B. Taylor.

TABLE OF CONTENTS

TABLE OF CONTENTS (CONTINUED)

LIST OF TABLES

LIST OF FIGURES

I. INTRODUCTION

Flutter is an aeroelastic dynamic instability where both bending and torsional components of a wing result in complex uncontrolled motion. Passive flutter suppression can be accomplished by increasing structural rigidity which requires additional weight. Recent advances in wing modeling and control theory have made active flutter suppression more attractive. Active flutter suppression to reduce the aeroelastic response of aircraft structures results in substantial weight savings, increased aircraft maneuverability, rider comfort and gust alleviation.

The state-space equations describing the flutter control problem represent the flexible structure, unsteady aerodynamics and actuator dynamics, and are usually of high order (~60 states). Modern control synthesis techniques applied to active flutter suppression, such as the standard linear quadratic Gaussian (LQG) solution, are of the same high order as the plant. Implementation requirements demand that the full-order control law be reduced or some how approximated. Active flutter control designs using the LQG approach and some form of control law model order reduction have been reported in Refs. 1 to 3. The control laws in Refs. 1 to 3 are all analog.

In this report, an alternative approach to modern control law synthesis is applied to the flutter suppression problem. The objective is to demonstrate the application of a digital active flutter control design methodology using optimal constrained dynamic compensators. The flutter control design is synthesized by minimizing a quadratic performance index defined by a weighted sum of mean-square steady state responses and control input as in the LQG approach. The difference is that the feedback control law is constrained to use only those measurements, y_k, which are practically available,

$$\underline{u}_k = K\underline{y}_k \tag{1}$$

$$\underline{y}_k = C\underline{x}_k + \underline{\gamma}_k \tag{2}$$

where $\underline{u}_k$, $\underline{x}_k$ and $\underline{\gamma}_k$ are the control, state and measurement noise vectors, respectively. The wind gusts which continually excite the wing, the measurement noise, $\underline{\gamma}_k$, from the sensors and the state initial condition errors are specified as part of the design model. Also included are the "to be designed" compensator dynamics,

$$\underline{z}_{k+1} = \beta_1 I\underline{z}_k + \beta_2 I\underline{u}_{c,k} \tag{3}$$

$$\underline{y}_{c,k} = I\underline{z}_k \tag{4}$$

The compensator dynamics are adjoined to the plant model as a completely controllable and observable stable system. The compensator controls are included in $\underline{u}_k$ and the perfect measurements of the compensator states (except for finite arithmetic) are included in $\underline{y}_k$.

There are a number of advantages to using the LQG output feedback approach combined with dynamic compensation. The order of the compensator can be specified by the designer subject to stabilizability constraints. For the flutter problem, dynamic compensation appears to be necessary to ensure stability at high dynamic pressure. The output feedback approach allows the designer to choose the simplest and easiest to implement control structure which achieves stability margins and low rms response. At the same time, dynamic systems which affect the control design, such as actuator dynamics and analog prefilters, can be included in the plant model without increasing control structure complexity.

The quadratic cost function used to represent design objectives is

specified in continuous-time along with the flutter model dynamics. The cost function and plant model are transformed to a discrete optimization problem using the sampled-data regulator approach. The resulting optimal output feedback digital control law is a direct digital design. The sample rate can be readily changed and new control gains obtained without having to adjust the continuous-time cost function weighting matrices to obtain comparable time-domain performance.

The computation delay that occurs in implementing the digital control system can be accommodated in the design by weighting control rate in the continuous-time cost function. Control rate weighting causes the optimal digital control law to use one-step delayed state information. The time frame that transpires after receiving the sampled filtered sensor measurement can be used to compute the control signal that is to be sent to the actuator channel at the beginning of the next time frame.

The optimal contrained dynamic compensator problem has been studied by researchers in Refs. 4 to 7. The necessary conditions for the control law to minimize the cost function are presented in Ref. 4 for the continuous case and Ref. 6 for the discrete case. Despite the many practical advantages of the approach, there are only a few serious studies of the application of optimal constrained dynamic compensators for continuous plants and none, that the authors are aware of, for discrete systems. There are at least three reasons which make the application of optimal output feedback design difficult. These difficulties are surmounted for the digital flutter suppression control law design presented in this report.

The most important reason is the lack of a fast, stable, reliable algorithm for iteratively solving the output feedback necessary conditions for relatively large order plants. Recently, in Ref. 8, the authors presented

a new algorithm for solving the necessary conditions, by computing a sequence of gains in Eq. 1 which converges to an optimal gain. This algorithm has been applied without difficulty to the digital flutter control law synthesis problem.

Three studies which determine analog output feedback control laws using dynamic compensators and cost functions somewhat similar to the one in this report are Refs. 9, 10, 11. Gradient search algorithms are used to minimize the cost function.

A comparison of the algorithm used in this report and a typical gradient search algorithm is given in Ref. 8. A comparison of the symplified version of the algorithm in this report (i.e. the case when α is forced to be 1.0 in Eq. 59) and typical gradient search algorithms is given in Ref. 12. Both references demonstrate the benefits offered by the algorithm in this report. Gradient search algorithms have the added difficulty that the search direction can lead to unstable closed-loop plants, a problem not encountered by the algorithm used in this report (for a sufficiently small α).

A second reason for optimal output feedback design difficulties, as reported in most of the references on optimal dynamic compensators, is that simply adjoining compensator dynamics to the plant and not weighting compensator controls or states in the cost function is unsatisfactory since the optimization process causes the unconstrained compensator gains to approach large values for continuous systems. To avoid this problem, Refs. 4 and 5, for example, include the compensator gains in the cost function using a modified version of compensator control weighting. A new approach is pursued for the flutter suppression control law design. The compensator states and controls are quadratically weighted in the cost function and an error term,

$$(\underline{z}_k - H_c \underline{x}_k)^T Q (\underline{z}_k - H_c \underline{x}_k) \tag{5}$$

is added to the cost function. The error term is an attempt to force the compensator states to estimate or observe chosen states of the plant. The globally optimal dynamic compensator for the case where the order of the compensator is n-ℓ (number of plant states - number of plant observations) is a reduced-order observer, (Ref. 7).

A third reason why optimal constrained dynamic compensator may be receiving little attention concerns the lack of any theoretical guarantee of good control system properties. Theoretical guarantees of phase and gain margins for the Linear Quadratic Regulator (LQR) full-state feedback control law are discussed in Ref. 13. The stability margins of the full-state feedback LQG approach can recover the stability margins of the LQR approach by using an input noise adjustment procedure described in Ref. 14. A flutter suppression control law designed using the LQG input noise adjustment method is presented in Ref. 1. Although a proof exists only for a full-order LQG control law, Section IVC numerically shows that improved stability margins can also be obtained for the discrete optimal constrained dynamic compensator approach. The improved stability margins are obtained by increasing the initial condition input covariance. Reference 10, which determined optimal constrained dynamic compensators by using a state reduced full-order Kalman filter as an initial guess and optimizing the gains in the reduced-order system, reached a similiar conclusion.

A. OVERVIEW OF THE REPORT

The state-space model for flutter control synthesis is discussed in Chapter II. The large order full-state evaluation model and the lower order design models obtained by residualization and balancing are presented. A baseline flutter model at $\bar{q}$ = 8.0 kPas, Mach = 0.9, is used throughout

the report. The control optimization problem is constructed in Chapter III. The sampled-data regulator approach is used. A continuous cost function and plant model are transformed to an equivalent discrete-time cost function and model. A single-rate, zero-order hold, digital control law design that accommodates computation delays is the desired objective. The steps in the algorithm used to solve the necessary conditions to minimize the cost function are presented in Chapter III.

Chapter IV presents the baseline control design parameters and closed-loop control law performance. The digital controller has a number of parameters which must be varied to trade off stability properties versus rms performance. The effects of varying the sampling rate, the prefilter time constant and control structure are investigated in Chapter V. As the control law must stabilize the wing for a wide range of flight conditions; Chapter VI contains stability properties and rms performance for a constant gain design and a gain scheduled design from $\bar{q}$ = 5.0 to 9.0 kPas. Chapter VII presents some recommendations and conclusions. Appendix A investigates relationships between compensators in this report and observers.

II. STATE-SPACE MODEL FOR FLUTTER CONTROL SYNTHESIS

The control law synthesis method presented in this report is used to synthesize an active flutter suppression control law for an aeroelastic wind-tunnel wing model. The geometry of the sweptback, canilevered wing model, along with sensor (accelerometer) and control surface locations, is shown in Fig. 1. The half-wing is scaled to flutter within the operational limits of the NASA Langley Transonic Wind-Tunnel. The wing has an electro-hydraulic servo-actuated trailing edge control surface. The surface hinge line is located at 80% of the local streamwise chord. The reaction torques of the actuator are constrained by a link to the main structural beam in the control pod section. The main structural beam is a single tapered aluminum bar construction with a cruciform cross section as shown in Fig. 1. The accelerometer and control surface locations were provided by NASA as part of the wing model.

A. AEROELASTIC MODEL OF THE WING

The mathematical model of wing deformation used in this report is discussed in detail in Ref. 15. Previous analyses of the problem have employed generalized coordinates, based on zero airspeed vibration modes or other fixed wing deformation shapes, from which generalized aerodynamic forces have been computed (Refs. 16-18). The model in Ref. 15 employs physical coordinates of bending and torsion of the wing structure directly, and uses constant influence coefficient matrices to describe the structural, inertial and aerodynamic forces.

The model is constrained to 7 node points in 2 degrees-of-freedom (vertical deflection and rotation in the flight direction). Two additional states are used for aileron deflection and an internal housing state linking the control surface to the main structural beam. The aeroelastic effects of the aileron are not neglected when the model is constructed, while the internal housing state has no

aeroelastic effect. The equations of motion are generated in terms of the forces and moments affecting the 15 degrees-of-freedom.

The state space model for the flutter problem can be written in standard form as

$$\begin{bmatrix} \dot{\underline{x}}_w \\ \dot{\underline{x}}_d \\ \dot{x}_a \\ \dot{\underline{x}}_g \end{bmatrix} = \begin{bmatrix} A_w & B_w & B_u & 0 \\ 0 & A_d & 0 & B_d \\ 0 & 0 & -A_a & 0 \\ 0 & 0 & 0 & A_g \end{bmatrix} \begin{bmatrix} \underline{x}_w \\ \underline{x}_d \\ x_a \\ \underline{x}_g \end{bmatrix} + \begin{bmatrix} 0 \\ 0 \\ A_a \\ 0 \end{bmatrix} \underline{u} + \begin{bmatrix} 0 \\ 0 \\ 0 \\ B_g \end{bmatrix} \eta \tag{6}$$

$$\underline{y} = \begin{bmatrix} C_w & E_w & D_w & 0 \end{bmatrix} \begin{bmatrix} \underline{x}_w \\ \underline{x}_d \\ x_a \\ \underline{x}_g \end{bmatrix} + \gamma_a \tag{7}$$

The state vector, $\underline{z}$, is partitioned as follows

$$\underline{x}_w^T = \begin{bmatrix} \overset{16}{\underline{z}_w^T}, & \overset{16}{\dot{\underline{z}}_w^T}, & \overset{15}{\underline{x}_{qa}^T} \end{bmatrix} \tag{8}$$

and is a 47x1 state vector. The 16x1 vector, $\underline{z}_w$, contains the 7 vertical deflections, h_i, 7 rotations, α_i, an internal housing state linking the control surface to the main structual beam, δ_h, and actuator position, δ_a. The 15x1 vector, $\underline{x}_{qa}$, is the unsteady life and moment vector. The 2x1 distrubance vector, $\underline{x}_d$, and 2x1 Dryden wind model vector, $\underline{x}_g$ are states for the external disturbance models which affect the unsteady aerodynamics. Equation 7 represents the accelerometer measurement. The parameter, γ_a, in Eq. 7 is accelerometer measurement disturbances modeled as zero-mean white noise with covariance V_a. The scalar, η, is a zero-mean white noise driving term for the Dryden wind model and has unit covariance.

The second-order Dryden wind model used to represent the Von Karmen power spectrum is

$$\frac{\xi_g}{\eta} = \sigma_{wg} \sqrt{\frac{L}{V_f}} \frac{\left(1 + \sqrt{3}\,\frac{L}{V_f}\,s\right)}{\left(1 + \frac{L}{V_f}\,s\right)^2} \tag{9}$$

σ_{wg} - root-mean-square (rms) gust velocity -0.3048 m/s

L - scale of turbulence or characteristic length -30.48 m

V_f - flight velocity, m/sec

The actuator dynamics are represented by a third-order transfer function given by (Ref. 1):

$$\frac{x_a}{u} = \frac{214}{s + 214} \tag{10}$$

$$\frac{\delta_a}{x_a} = \frac{89450}{s^2 + 179.45s + 89450} \tag{11}$$

The first-order pole in Eq. 10 is modeled as the state x_a in Eq. 6. The second-order polynomial in Eq. 11 is embedded in the wing model state-space representation. The parameter A_a in Eq, 6 has the value 214.0 as shown in Eq. 10. The matrices A_g and B_g in Eq. 6 are determined from the state-space representation of Eq. 9.

B. MODEL STATES CAUSED BY THE CONTROL STRUCTURE

The accelerometer signal used for feedback senses low and high frequency wing motion as well as noise. Flutter is predicted at a dynamic pressure of 5.36 kPa and a frequency near 50 rad/sec (the lowest wing motion frequency in the wing model). Digital control laws can have improved performance if a properly chosen analog prefilter is used to suppress high frequency disturbances in the sensor output before the sensor output is sampled, (Refs. 19 and 20).

A first-order prefilter with the transfer function

$$y_f = \frac{a}{s + a} y \tag{12}$$

is used in the digital control law design. If a full state feedback linear quadratic regulator control system is designed, then all plant states, including prefilter states, would have to be measured for feedback, however, the use of output feedback does not require the measurement of all the states and does not neglect the prefilter dynamics. The baseline value for the prefilter pole, a, is chosen to be near the flutter frequency, (-50.0 rad/sec). The prefilter also serves to suppress stable high frequency wing deformation modes which are aliased near the flutter mode frequency after sampling.

The digital control law uses dynamic compensation to improve closed-loop stability and performance. The order of the dynamic compensator is arbitrarily chosen. The compensator states are introduced in the model as stable dynamics with perfect control and noise free observation,

$$\dot{\underline{z}} = -\beta I \underline{z} + I \underline{u}_c \tag{13}$$

$$\underline{y}_c = I \underline{z} \tag{14}$$

A digital control law requires a finite amount of computation time to output a control command after measurements are obtained. Neglecting the computation delay can have adverse effects, including instability, on closed-loop performance. An effective method for accommodating the computation delay in the Linear Quadratic Regulator design approach is to weight control rate in the quadratic cost function, Ref. 21. The optimization problem is solved by including control rate dynamics in the continuous-time wing model.

$$\dot{u} = v \tag{15}$$

Weighting v in the cost function weights control rate. The discrete control law that results from using Eq, 15 requires that the control actuator command applied at time t_k be computed during the time interval, $t_k - t_{k-1}$, using the accelerometer measurement obtained at the sampling instant, t_{k-1}.

C. MODEL-ORDER REDUCTION AND THE DESIGN MODEL

The complete wing modwl has 47 states to describe wing motion, 5 states for disturbance and actuator dynamics and $2+\sigma$ states for the control law with dynamic compensation (1 prefilter state, 1 control rate state, and σ compensator states) for a total of $54+\sigma$ states. The complete wing model is used to evaluate control performance. A block diagram of the wing model and discrete control law is shown in Fig. 2.

The design model is a state-space representation of the wing that is smaller in dimension than the evaluation wing model. The design model is used in the active flutter control optimization problem to determine the feedback gains in the control law. A lower dimension design model reduces the cost of control design without significantly compromising closed-loop performance, as will be shown.

The design model is obtained by residualizing the high frequency and very stable modes in the 47 state wing model. The residualization procedure begins by computing the eigenvalues and eigenvectors of the 47 state wing model. The eigenvalues are shown in Table 1 for the baseline ($\bar{q}$ = 8.0 kPa) flight condition. A real transformation matrix, T, is computed by arranging eigenvectors columnwise. If an eigenvector is complex, the real part is placed as one column and the imaginary part is placed as the next column in T,

$$A_w \underline{x}_i = \lambda_i \underline{x}_i \tag{16}$$

$$T = \left[\text{Real}(\underline{x}_1) \quad \text{Imag}(\underline{x}_1) \quad \ldots \right], \quad \lambda_1 = a_1 + j\, b_1 \tag{17 a,b}$$

The transformed wing model is block diagonal and results in the model representation of the wing dynamics. The eigenvalues are ordered as shown in Table 1,

$$T^{-1}A_w T = \begin{bmatrix} a_1 & b_1 & 0 & 0 & \cdot & \cdot & \cdot \\ -b_1 & a_1 & & & & & \\ 0 & 0 & a_2 & b_2 & & & \\ \cdot & & -b_2 & a_2 & \cdot & & \\ \cdot & & & & \cdot & \cdot & \\ \cdot & & & & & \cdot & \\ & & & & & & a_n \end{bmatrix} = \bar{A}_w \tag{18}$$

Complex eigenvalues form 2x2 diagonal blocks in $\bar{A}_w$, while real eigenvalues are scalars on the diagonal.

The transformed model wing model, ($\bar{A}_w$, $\bar{B}_u$, $\bar{B}_w$, $\bar{C}_w$) is partitioned as follows

$$\begin{bmatrix} \dot{\bar{x}}_{w1} \\ \dot{\bar{x}}_{w2} \end{bmatrix} = \left[\begin{array}{c|c} \bar{A}_{11} & 0 \\ \hline 0 & \bar{A}_{22} \end{array}\right] \begin{bmatrix} \bar{x}_{w1} \\ \bar{x}_{w2} \end{bmatrix} + \begin{bmatrix} \bar{B}_{u1} \\ \bar{B}_{u2} \end{bmatrix} x_a + \begin{bmatrix} \bar{B}_{w1} \\ \bar{B}_{w2} \end{bmatrix} \underline{x}_d \tag{19}$$

$$y = \begin{bmatrix} \bar{C}_{w1} & \bar{C}_{w2} \end{bmatrix} \begin{bmatrix} \bar{x}_{w1} \\ \bar{x}_{w2} \end{bmatrix} + D_w \; x_a + E_w \; \underline{x}_d + \gamma_a \tag{20}$$

The $\bar{x}_w$ states in Eq. 19 are equal to $T^{-1}x_w$. The derivatives of the high frequency and very stable states, $\bar{x}_{w2}$ are assumed to be zero and are eliminated from the model, yielding,

$$\dot{\bar{x}}_{w1} = \bar{A}_{11}\,\bar{x}_{w1} + \bar{B}_{u1}\,x_a + \bar{B}_{w1}\,\underline{x}_d \tag{21}$$

$$y = \bar{C}_{w1}\,\bar{x}_{w1} + (D_w - \bar{C}_{w2}\bar{A}_{22}^{-1}\bar{B}_{u2})\,x_a + (E_w - \bar{C}_{w2}\bar{A}_{22}^{-1}\bar{B}_{w2})\,\underline{x}_d + \gamma_a \tag{22}$$

The control design model partition is shown in Table 1 and uses all states up to and including those which govern the actuator dynamics. The control law produces unsatisfactory closed-loop performance if the actuator dynamics are residualized or neglected. A second, higher order evaluation model shown in Table 1, is used to compute Bode plots and Nyquist plots using the program DIGIKON, Ref. 22. The version of DIGIKON employed has a maximum limit on the number of states allowed in the plant model.

The residualized procedure used for the wing model is also used to reduce the 4 state dynamical representation of the disturbances $\underline{x}_d$ and $\underline{x}_g$ to one state in the design model, $\bar{x}_g$. The models for $\bar{x}_g$, $\underline{x}_d$, x_a and $\underline{x}_g$ are numerically balanced, using results from Ref. 23, to improve computational accuracy for the design and evaluation models.

The balancing procedure was also investigated as an alternative method for reducing the order of wing model. The control designs using the balanced reduced-order models were acceptable, but were poor in comparison to the control designs obtained using residualization. Closed-loop eigenvalue locations for the design and evaluation models were more dispersed for the balanced reduced-order design models.

Grouping all the models together, the instantaneous measurements are

$$\begin{bmatrix} y_F \\ \underline{y}_c \\ u \end{bmatrix} = \overbrace{\left[\begin{array}{cccc|cc} 0 & 0 & 0 & 1 & 0 & 0 \\ \hline 0 & 0 & 0 & 0 & I & 0 \\ 0 & 0 & 0 & 0 & 0 & 1 \end{array}\right]}^{C_P} \begin{bmatrix} \bar{\underline{x}}_{wl} \\ x_a \\ \bar{x}_g \\ x_f \\ \underline{z} \\ u \end{bmatrix} \tag{23}$$

and the $14+\sigma$ order control design model is:

$$\begin{bmatrix} \dot{\bar{x}}_{wl} \\ \dot{x}_a \\ \dot{\bar{x}}_g \\ \dot{x}_f \\ \dot{\underline{z}} \\ \dot{u} \end{bmatrix} = \overbrace{\left[\begin{array}{cccc:cc} \bar{A}_{11} & \bar{B}_{ul} & \bar{B}_w & 0 & 0 & 0 \\ 0 & -A_a & 0 & 0 & 0 & A_a \\ 0 & 0 & \bar{A}_g & 0 & 0 & 0 \\ a\bar{C}_{wl} & a\bar{D} & a\bar{E} & -a & 0 & 0 \\ \hdashline 0 & 0 & 0 & 0 & -\beta I & 0 \\ 0 & 0 & 0 & 0 & 0 & 0 \end{array}\right]}^{A} \left.\begin{bmatrix} \bar{x}_{wl} \\ x_a \\ \bar{x}_g \\ x_f \\ \underline{z} \\ u \end{bmatrix}\right\} \underline{x}_p$$

$$+ \overbrace{\left[\begin{array}{cc} 0 & 0 \\ 0 & 0 \\ 0 & 0 \\ 0 & 0 \\ \hdashline I & 0 \\ 0 & 1 \end{array}\right]}^{B} \begin{bmatrix} \underline{u}_c \\ v \end{bmatrix} + \overbrace{\left[\begin{array}{cc} 0 & 0 \\ 0 & 0 \\ \bar{B}_g & 0 \\ 0 & a \\ \hdashline 0 & 0 \\ 0 & 0 \end{array}\right]}^{E} \left.\begin{bmatrix} \eta \\ \gamma_a \end{bmatrix}\right\} \underline{w} \qquad (24)$$

III. ACTIVE FLUTTER SUPPRESSION OPTIMIZATION PROBLEM

The control design optimization problem for synthesizing an active flutter suppression control system is presented in this chapter. The control design uses an infinite-time quadratic cost function to represent design objectives. The quadratic weights in the continuous-time cost function are chosen by the designer. The cost function and plant model are transformed to a discrete optimization model by assuming the control inputs can only change at equally spaced sample points in time. The compensator states and plant states are cross-weighted in the cost function in an attempt to make the compensator state estimate, or "observe", specified wing model modes. The discrete control structure is constrained to use feedback of only specified states. The necessary conditions the constrained feedback gain must satisfy in order to minimize the discrete cost function is detailed. An algorithm for determining a gain which satisfies the necessary conditions, resulting in a local minimum, is presented.

A. CONTINUOUS-TIME OPTIMIZATION PROBLEM

The continuous quadratic cost function begins with the following standard quadratic form,

$$J = \frac{1}{2} E\left[\int_o^\infty \left\{ \begin{bmatrix} \bar{x}_{wl}^T & x_a & \bar{x}_g & x_f & z^T & u \end{bmatrix} \begin{bmatrix} Q_l & & & & & 0 \\ & 0 & & & & \\ & & 0 & & & \\ & & & 0 & & \\ & & & & Q_c & \\ 0 & & & & & R \end{bmatrix} \begin{bmatrix} \bar{x}_{wl} \\ x_a \\ \bar{x}_g \\ x_f \\ z \\ u \end{bmatrix} + \begin{bmatrix} u_c^T & v \end{bmatrix} \begin{bmatrix} R_c & 0 \\ 0 & R_v \end{bmatrix} \begin{bmatrix} u_c \\ v \end{bmatrix} \right\} dt \right] \quad (25)$$

At this state in development, the above cost function is different from previous attempts to design dynamic compensators using output feedback because both z and u_c are weighted.

If $\underline{u}_c$ is not weighted in the cost function, the continuous-time optimization problem can become singular. The R_c matrix can be zero in the discrete-time optimization problem without causing the singularity problem, but the compensator gains can still become very large.

A solution to the output feedback optimization problem using Eq. 25 is somewhat ambiguous since the compensator states have no intuitive interpretation. Optimal designs using the Kalman filter, Ref. 19, or observer, Ref. 7, use compensators with states that have clearly defined roles as observers of plant states. A discussion of the problem of when is a compensator an observer and what does it observe is discussed in Appendix A. The global optimum for the optimization problem with compensator states having arbitrarily specified order less than n-ℓ remains unsolved.

A heuristic approach is taken for the active flutter suppression control design. The approach successfully accommodates algorithm convergence difficulties, provides compensator states with an intuitive interpretation and contribures toward improving control law robustness. A new term, represented in Eq. 5, is added to the cost function as follows,

$$J = \frac{1}{2} E\left[\int_o^\infty \left\{ \left[\bar{\underline{x}}_{wl}^T x_a \; \bar{x}_g \; x_f \; \underline{z}^T u\right] \begin{bmatrix} (Q_1+H_c^T Q H_c) & \cdots & -H_c^T Q & 0 \\ \vdots & & & \\ -QH_c & & (Q_c+Q) & 0 \\ 0 & & 0 & R \end{bmatrix} \begin{bmatrix} \bar{\underline{x}}_{wl} \\ x_a \\ \bar{x}_g \\ x_f \\ \underline{z} \\ u \end{bmatrix} \right.\right.$$

$$\left.\left. + \left[\underline{u}_c^T \; v\right] \begin{bmatrix} R_c & 0 \\ 0 & R_v \end{bmatrix} \begin{bmatrix} \underline{u}_c \\ v \end{bmatrix} \right\} dt \right] \qquad (26)$$

Q and H_c are chosen to be full rank. The new term has the following properties:

- As Q is increased, the compensator states are interpreted as more closely following (observing) $H_{c\bar{x}_{wl}}$. H_c can be arbitrarily chosen subject to the rank condition.
- If Q is nonzero, the algorithm to be discussed in Section III-D converges to a control law where the compensator and plant are coupled, even if the starting stabilizing gain is uncoupled. When Q is zero, an uncoupled starting stabilizing gain (K_y, K_u, and $\bar{K}_c$ are zero matrices in Eq. 31) causes the algorithm to converge to an uncoupled gain which satisfies the necessary conditions.
- The solution with and without Q is non-unique when compensator states are included in the plant model. Different starting gains converge to different local minimums. The different compensator designs at local minimums are not necessarily related by a transformation matrix (Ref. 7).
- A simple root locus using the wing model at 8.0 kPa (the design flight condition) demonstrated that the wing model at 8.0 kPa cannot be stabilized using only the accelerometer measurement. The plant and compensator must be coupled to minimize the cost function for the active flutter suppression problem.
- The new term in the cost function is similiar to techniques used in explicit model following approaches, Ref. 24 and 25. The difference is that the compensator dynamics (i.e. the model dynamics in explicit model following parlance) are allowed to be changed by the optimization process.

The continuous problem is transformed to a discrete problem using the sampled-data regulator as discussed in the next section.

B. DISCRETE OPTIMIZATION PROBLEM

The controls $\underline{u}_c$, v and u are assumed to be constant over the fixed sampling interval, Δt. The piecewise constant controls allow the design model shown in Eq. 23, and the cost function shown in Eq. 26, to be transformed to an equivalent sampled-data regulator problem, (Ref. 26),

$$\overbrace{\begin{bmatrix} \underline{x}_p \\ \underline{z} \\ u \end{bmatrix}}^{\underline{x}}_{k+1} = \overbrace{\begin{bmatrix} \Phi_p & 0 & \Gamma_p \\ 0 & \beta_1 I & 0 \\ 0 & 0 & I \end{bmatrix}}^{\Phi} \begin{bmatrix} \underline{x}_p \\ \underline{z} \\ u \end{bmatrix}_k + \overbrace{\begin{bmatrix} 0 & (\sim 0) \\ \beta_2 I & 0 \\ 0 & \Delta t I \end{bmatrix}}^{\Gamma} \overbrace{\begin{bmatrix} \underline{u}_c \\ v \end{bmatrix}_k}^{\underline{u}} + \Gamma_w \underline{w}_k \tag{27}$$

$$\begin{bmatrix} y_f \\ \underline{y}_c \\ u \end{bmatrix} = \overbrace{\begin{bmatrix} C_p & 0 & 0 \\ 0 & I & 0 \\ 0 & 0 & 1 \end{bmatrix}}^{C} \begin{bmatrix} \underline{x}_p \\ \underline{z} \\ u \end{bmatrix}_k + \underline{\gamma}_k \tag{28}$$

$$J_N = \frac{1}{2N} \; E\left[\sum_{k=0}^{N} \left\{ \underline{x}^T \hat{Q} \, \underline{x} + 2 \, \underline{x}^T \hat{M} \, \underline{u} + \underline{u}^T \hat{R} \, \underline{u} \right\} \right] \quad N > 0 \tag{29}$$

$$J = \lim_{N \to \infty} J_n \tag{30}$$

The state $\underline{x}_p$ in Eq. 27, as shown in Eq. 23, is equal to the state vector $\begin{bmatrix} \underline{x}_{wl}^T & x_a & \underline{x}_g & x_f \end{bmatrix}^T$. The upper right partition of Γ in Eq. 27 is assumed to be zero. If this assumption is not used, the implied continuous-time implementation for $\underline{u}(t)$ would be a triangular data hold. The control, $\underline{u}(t)$, is constant over the sampling instant if Γ is modified as shown. A white noise term, $\underline{\gamma}_k$, with covariance, V, is added to the discrete measurements and is treated as a design parameter.

The class of control laws considered are restricted to be of the form

$$\begin{bmatrix} \underline{u}_c \\ v \end{bmatrix}_k = \overbrace{\begin{bmatrix} K_y & K_\Phi & K_u \\ \bar{K}_f & \bar{K}_c & K_v \end{bmatrix}}^{-K} \begin{bmatrix} y_f \\ \underline{z} \\ u \end{bmatrix}_k \tag{31}$$

Defining the variables

$$\Phi_c = \beta_1 I + \beta_2 K_\Phi \tag{32}$$

$$\Phi_u = I + \Delta t K_v \tag{33}$$

$$\Gamma_c = \beta_2 K_y \tag{34}$$

$$\Gamma_u = \beta_2 K_u \tag{35}$$

$$K_f = \Delta t \bar{K}_f \tag{36}$$

$$K_c = \Delta t \bar{K}_c \tag{37}$$

The implementable form for the control law with the compensator is

$$\underline{z}_{k+1} = \Phi_c \underline{z}_k + \Gamma_c y_{f,k} + \Gamma_u \underline{u}_k \tag{38}$$

$$\underline{u}_{k+1} = \Phi_u \underline{u}_k + K_f y_{f,k} + K_c \underline{z}_k \tag{39}$$

C. NECESSARY CONDITIONS FOR OPTIMALITY

One final problem must be resolved before the necessary conditions for optimality for the output feedback probelm can be determined. The cost in Eq. 29 minimizes the average long term stochastic performance of the plant. State and control initial condition errors are averaged to zero as N increases and do not affect the control design. In contrast to stochastic output feedback, the LQG problem and the deterministic optimal output feedback approach in Ref. 4, are primarily concerned with driving initial conditions errors to

zero; another desirable control objective. A final modification to the quadratic cost function is constructed where minimum stochastic performance and fast response (and as is shown later, robustness) can be traded off against each other,

$$\underline{x}_k = \Phi_{CL}^{k}\,\underline{x}_o + \sum_{i=0}^{k-1} \Phi_{CL}^{k-i-1}\,(\Gamma_w\,\underline{w}_i - \Gamma\,K\,\underline{\gamma}_i) = \underline{x}_{tk} + \underline{x}_{sk} \qquad (40\ a)$$

$$\underline{u}_k = -K\,\underline{y}_k = -\,K\,C\,\underline{x}_{tk} - K(C\,\underline{x}_{sk} + \underline{\gamma}_k) = \underline{u}_{tk} + \underline{u}_{sk} \qquad (40\ b)$$

$$J(K) = \frac{1}{2}\,(J_t + J_s) \qquad (41)$$

$$J_t = \sum_{k=0}^{\infty} \underline{x}_{tk}^T\,\hat{Q}\,\underline{x}_{tk} + 2\,\underline{x}_{tk}^T\,\hat{M}\,\underline{u}_{tk} + \underline{u}_{tk}^T\,\hat{R}\,\underline{u}_{tk} \qquad (42)$$

$$J_s = \lim_{N\to\infty} \frac{1}{N+1}\,E\left[\sum_{k=0}^{N} \underline{x}_{sk}^T\,\hat{Q}\,\underline{x}_{sk} + 2\,\underline{x}_{sk}^T\,\hat{M}\,\underline{u}_{sk} + \underline{u}_{sk}^T\,\hat{R}\,\underline{u}_{sk}\right] \qquad (43)$$

The plant response is separated into the transient component, $\underline{x}_{tk}$, and the stochastic component, $\underline{x}_{sk}$, as shown in Eq. 40 a. The feedback control law is similarly partitioned into the transient, $\underline{u}_{tk}$, and the stochastic, $\underline{u}_{sk}$, components. J_t is the transient cost with noise sources set to zero while J_s is the average stochastic cost. The objective is to determine the output feedback gain K in Eq. 40 b which minimizes the average cost shown in Eq. 41. The necessary conditions for minimizing J(K) are straightforward if the quadratic weights in J_t and J_s are equal. The tradeoff between J_t and J_s is accomplished by changing X_o, the covariance of the plant state initial condition.

For the plant dynamics shown in Eq. 23, the feedback gain constraint shown in Eq. 31, and the following conditions.

$$E\left[\underline{w}_k\right] = 0.0 \qquad E\left[\Gamma_w\,\underline{w}_k\,\underline{w}_j^T\,\Gamma_w^T\right] = W\delta_{kj} \qquad (44\ a, b)$$

$$E\left[\underline{\gamma}_k\right] = 0.0 \qquad E\left[\underline{\gamma}_k\,\underline{\gamma}_j^T\right] = V\delta_{kj} \qquad (45\ a, b)$$

$$E\left[\underline{w}_k \underline{\gamma}_j^T\right] = E\left[\underline{w}_k \underline{x}_0^T\right] = E\left[\underline{v}_k \underline{x}_0^T\right] = 0.0 \tag{46}$$

$$E\left[\underline{x}_0 \underline{x}_0^T\right] = X_0 \tag{47}$$

The cost in Eq. 41 can be rewritten as follows, (Ref. 8),

$$J(K) = \tfrac{1}{2} \text{ tr } \left\{P(W + X_0)\right\} + \tfrac{1}{2} \text{ tr } \left\{K^T(\Gamma^T P \Gamma + \hat{R})KV\right\} \tag{48}$$

The matrix, P, satisfies the Riccati-like equation,

$$P = \Phi_{CL}^T P \Phi_{CL} + C^T K \hat{R} K C + \hat{Q} - \hat{M} K C - C^T K^T \hat{M}^T \tag{49}$$

Φ_{CL} is the stable closed-loop plant matrix,

$$\Phi_{CL} = \Phi - \Gamma K C \tag{50}$$

The matrices Φ, Γ and C are defined in Eq. 27.

The necessary conditions for J(K) to have a minimum are derived in Ref. 8. There must exist a gain, K, so that Φ_{CL} is stable. The gain, K, must satisfy Eq. 49 and the following

$$S = \Phi_{CL} S \Phi_{CL}^T + (W + X_0) + \Gamma K V K^T \Gamma^T \tag{51}$$

$$\left[\Gamma^T P \Gamma + \hat{R}\right] K \left[C S C^T + V\right] = \left[\Gamma^T P \Phi + \hat{M}^T\right] S C^T \tag{52}$$

A few comments are

- If W and V are zero matrices, the necessary conditions are the solution to the deterministic output feedback problem, J_t, with J_s zero.
- If X_0 is a zero matrix, the necessary conditions are the solution to the stochastic output feedback problem, J_s, with J_t zero, and S is the covariance matrix for $E\left[\underline{x}_k \underline{x}_k^T\right]$.

- The covariance, X_0, performs the same function as adding pseudonoise to the plant to improve closed-loop performance.

An algorithm to compute the optimal K which satisfies Eqs. 49, 51 and 52 is given in Ref. 8. An optimal gain exists provided an initial stabilizing gain exists, Γ and C have full rank, $m \leq n$, $\ell \leq n$ and

$$W > 0 \tag{53}$$

$$\hat{Q} > 0 \tag{54}$$

The above conditions guarantee convergence. The algorithm may still converge if the conditions are not satisfied as in the case in this report.

D. A PRACTICAL CONVERGENT ALGORITHM FOR DISCRETE OPTIMAL OUTPUT FEEDBACK

Step 1: Choose K_0 so that $\Phi_{CL} = \Phi - \Gamma K_0 C$ is stable, $\alpha_0 \varepsilon (0,1]$, $z > 1$, j an integer ≥ 1 and set $i = 0$.

Step 2: Solve Eq. 51 for S using K. The Bartels-Stewart algorithm in Ref. 27 is recommended.

Step 3: Solve Eq. 49 for P using K_i.

Step 4: Invert the symmetric matrices:

$$\hat{P} = \Gamma^T P \Gamma + \hat{R} \tag{55}$$

$$\hat{S} = CSC^T + V \tag{56}$$

using Cholesky decomposition. If the symmetric matrices $\hat{P}$ and $\hat{S}$ are not positive definite, go to Step 8.

Step 5: Compute K_{NEW}, $d(K_i)$

$$K_{NEW} = \hat{P}^{-1}\left[\Gamma^T P \Phi + \hat{M}^T\right] SC^T \hat{S}^{-1} \tag{57}$$

$$d(K_i) = K_{NEW} - K_i \tag{58}$$

Step 6: Compute K_{i+1}

$$K_{i+1} = K_i + \alpha_i d(K_i) \tag{59}$$

Step 7: Evaluate the cost function, J_i, using Eq. 48. If i = 0, set i to 1, $\alpha_{i+1} = \alpha_i$ and go to Step 2. If J_i is negative, go to Step 8. If $J_i - J_{i-1}$ is negative, go to Step 9, otherwise, go to Step 8.

Step 8: Decrease α_i using z: $\alpha_i = \alpha_i/z$

Go back to a previous stabilizing gain

$$K_i = K_{i-j}, \quad d(K_i) = d(K_{i-j}) \tag{60 a,b}$$

Compute

$$K_{i+1} = K_i + \alpha_i d(K_i) \tag{61}$$

Set $\alpha_{i+1} = \alpha_i$, i = i+1 and go to Step 2.

Step 9: Compute $\frac{\partial J}{\partial K}(K_i)$

$$\frac{\partial J}{\partial K}(K_i) = \hat{P}K_i\hat{S} - \left[\Gamma^T P\Phi + \hat{M}^T\right] SC^T \tag{62}$$

If $\left\| \frac{\partial J}{\partial K}(K_i) \right\|$ and $(J_i - J_{i-1})/J_i$ are less than some convergence criterion stop, otherwise set $\alpha_{i+1} = \alpha_i$, i = i+1, and go to Step 2.

Reference 8 derived the property that there exists an $0 < \alpha \leq 1$ such that the algorithm is stable. The algorithm uses a number of checks to determine if the current value of α is too large and reduces α accordingly. Numerical experience indicates that the algorithm converges fastor for values of α closer to 1.0.

IV. DIGITAL CONTROL DESIGN

This chapter presents the design values for the baseline control system. The digital control design is determined by choosing elements in Q, R, W, X_o and V, finding an initial stabilizing gain and computing the locally optimum, K, using the design wing model. The control design is evaluated using the evaluation wing model to obtain rms response for states and controls. Nyquist plots are determined using a lower dimension evaluation model. Adjustments are made to design elements until a desired performance tradeoff is obtained.

A. PROCEDURE FOR COMPUTING AN INITIAL STABILIZING GAIN

The dynamic compensator makes it difficult to apply output feedback stabilization procedures to the flutter control problem. A straightforward approach is presented that successfully determines an initial stable gain for the flutter problem.

Taking advantage of the block diagonal form of the flutter model, the unstable flutter mode in the model is forced stable by adjusting the 2x2 block parameters. K_v in Eq. 31 is easily chosen to stabilize Φ_u and β in Eq. 13 is set to 10. With all gains but K_v zero, Φ_{CL} is stable and a new preliminary gain can be determined with the algorithm and the modified wing model.

The process is repeated using the new preliminary stabilizing gain and perturbing the flutter mode in the direction of the true value. If the control design is relatively insensistive to the artifically induced plant parameter variations, a valid stabilizing gain can be iteratively computed in a few steps. Three iterations were used for the wing model.

An alternative approach is to start the design at a low dynamic pressure flight condition where the flutter mode is stable. Increasing $\bar{q}$ iteratively and using the previous gain from the algorithm for each increase in $\bar{q}$ also results in a stabilizing gain at the desired flight condition.

B. DESIGN VARIABLES AND OBJECTIVES

The optimal output feedback design problem for flutter suppression has a number of design variables which must be chosen by the designer. The wing model is similar to (but not the same as) the wing model in Refs. 1 and 10. The control performances in Refs. 1 and 10 form reasonable objectives for specifying the control design variables and are shown in Table 2. The differences between the approaches are

- Digital design in this report verses analog designs in Refs. 1 and 10.
- 4 compensator + 1 prefilter + 1 control state in this report versus 4 compensator + 1 prefilter state in Ref. 1 versus 4 compensator states in Ref. 10.
- This report, Ref. 1 and Ref. 10 each use different plant model orders for the design wing models.

The Dryden wind model shown in Eq. 9 disturbs the dynamics for both references.

The parameter design variables are the prefilter time constant, the sampling time Δt, the accelerometer measurement noise covariance, the cost function weights, Q_1, Q_c, Q, R, R_c, R_v and the state initial condition matrix, X_o. Structural design variables are the order of the compensator, the compensator observation matrix, H_c, and the timing of the y_f observation.

C. DESIGN VALUES

Using Refs. 1 and 10 as guidelines, the order of the compensator, σ, is chosen to be four. The matrix, H_c, is chosen so that the first two compensator states "observe" the unstable flutter mode in Table 1 and the third and fourth compensator states "observe" the second mode in Table 1. The (4 x 10) matrix, H_c, is chosen with the plant states expressed in reduced-order model coordinates as shown in Eq. 26. Elements in H_c are simply zeroes and ones.

As a general rule, if poles and zeroes are "close", the pole is usually "close" to being uncontrollable or unobservable. Modes 3 and 4, in Table 1, represent stable modes that are only moderately affected by the control design as shown in Table 3. Increasing the order of the compensator to account for modes 3 and 4 is not required.

The sampling rate is chosen to be 200 samples/sec. Plant modes with natural frequencies above 628.3 rad/sec are aliased by the sampler. The aliased frequencies for these modes are shown in the second column of Table 3. The mapped poles in Table 3 are determined by first computing Φ_{CL} for the full order closed-loop evaluation model, computing the discrete closed-loop poles, then mapping the discrete poles back into the s-domain using the natural log,

$$\text{Discrete pole} \qquad \lambda = a + jb \tag{63}$$

$$\text{Discrete pole} \qquad \lambda = \sqrt{a^2 + b^2}\ e^{j\tan^{-1}b/a} \tag{64}$$

$$\text{Mapped Discrete pole} \qquad \frac{1}{\Delta t} \ln \lambda = \frac{1}{\Delta t} \ln \left(\sqrt{a^2 + b^2}\right) + j \frac{1}{\Delta t}\tan^{-1}b/a \tag{65}$$

Covariance values and quadratic weights chosen for the design are shown in Table 4. The covariance, X_u, is the input control position initial condition covariance. The covariance, X_u, is the eleventh diagonal element in the X_o covariance matrix shown in Eq. 47. The covariance X_u is defined as $X_u = E\left\{x_a^2\right\}$. Table 5 shows that increasing X_u increases gain margins and phase margins but also increases control surface activity. A compromise must be reached between the conflicting objectives of good stability margins and low control surface activity. If the control surface activity is high, moderate gusts can cause the surface to saturate quickly, the design may become sensitive to unmodeled accelerometer noise disturbances and the control system may become susceptible to limit cycling. The design

for X_u = 0.10 in Table 5 is selected as the compromise value. The gain margins, phase margins and covariance activity in Table 5 compare favorably to the analog designs in Table 2.

Table 5 shows that the input noise adjustment procedure is capable of improving stability margins for the output feedback compensator design synthesis technique used in this report for the wing model. Improving stability margins increases control surface activity. Adjusting the input noise affects both the compensator and the output feedback gains. The implication is that artificial input noise variation may benefically affect stability margins for any design using the output feedback design approach discussed in Chapter III (with or without compensator states).

The Nyquist diagrams for the three control laws in Table 5 are presented in Fig. 3 and show the progressive increase in phase and gain margins. A Bode plot of the reduced-order plant plus the X_u = 1.0 control law design is presented in Fig. 4. The rapid changes at 415 rad/sec and 163 rad/sec are caused by the zeros near these frequencies as shown in Table 1. The bandwidth in Table 5 is the highest frequency in the Bode plot at which the gain is greater than -6B.

Table 6 shows the variance values for deflection and rotation of the 7 mass bodies which comprise the wing model for a 0.305 m/s (1 ft.) gust input. The variances increase from the fuselage to the wing tip but have acceptable values.

D. NUMERICAL EXPERIENCE

Numerical experience with the algorithm and the flutter control problem with dynamic compensation verified that the baseline control design performance given in Table 5 is probably a local minimum. Different starting gains converge to different designs with different rms performance. The design in

Table 5 could probably be improved by starting the algorithm at different stable gains and comparing performance. Theoretical and numerical procedures which guarantee uniqueness is an area of investigation recommended in Chapter VII.

Figure 5 shows a typical convergence pattern of the output feedback algorithm. The largest improvements in the cost function occur within 10 iterations. Values for the algorithm's α parameter, defined in Section III-D, vary between 0.2 and 0.05 depending on the weighting and covariance values.

In the next section, design parameters are varied and the effect on performance is tabulated. Whenever possible, the starting gain is fixed at the same value for each variation.

V. EFFECT OF VARYING CONTROL PARAMETERS AND STRUCTURE

In this chapter, the effects of lowering the sample rate, varying the prefilter time constant and altering the control structure from a "one-step prediction" to an "update" implementation are investigated. The starting gain column in the Tables indicates if the starting stabilizing gain is the same as the starting gain in the baseline design. If the gains are not the same, the starting stabilizing gain is the locally optimum gain obtained in the previous variation being investigated.

A. SAMPLE RATE VARIATION

Slower sample rates lower the requirements for computer specifications, computer code efficiency and A/D; D/A converters. The effect of progressively lowering the sample rate from 200 samples/sec to 100 samples/sec is shown in Table 7. The complexities of making meaningful comparisons, as well as the optimization's propensity for advantageous reconfiguration is evident in the Table. The control rms response improves with lower sample rates for fixed X_u, but gain and phase margins degrade, particularly at the higher frequency crossover points. The X_u covariance is increased to 0.25 for the 160 sample/sec design in an attempt to match δ_{rms} response with the 200 sample/sec design. The degradation in high frequency gain and phase margin at the lower sample rate is evident. Sample rates below 140 samples/sec appear to have questionable performance.

B. PREFILTER POLE VARIATIONS

Analog flutter control laws in Ref. 28 used first order analog prefilters in all the designs reported. Values for the prefilter pole ranged from -5.0 to -20.0. The control laws in Ref. 28 use two sensors for feedback. Torsional wing motion can be made better observable with two sensors.

Lower prefilter poles for the one accelerometer sensor used in this report degrade rms response for the control surface, but improve gain and phase margins (except for the high frequency gain margin) as shown in Table 8. The best compromise appears to be to reduce the magnitude of the prefilter pole until δ_{rms} response is marginally acceptable. Although not studied in this application, a wash-out filter (s/s+b) should be incorporated with the prefilter to suppress low frequency motion of the wing caused by aircraft maneuvers.

C. ALTERNATE CONTROL STRUCTURE

The control law shown in Fig. 2 is purposely designed so that $\underline{u}_k$ uses the $\underline{y}_{f,k-1}$ measurement for feedback. The control $\underline{u}_k$, by definition, is to be written by the onboard computer to the actuator output port at the time instant t_k. A one sample time period, Δt, occurs in real time in the onboard computer between receiving $\underline{y}_{f,k-1}$ from the measurement input port and writing $\underline{u}_k$ to the actuator output port. The Δt time period can be used to compute $\underline{u}_k$ using Eqs. 38 and 39.

Consider changing Eq. 28 so that $\underline{y}_{f,k+1}$ is assumed to be the measurement at t_k,

$$\underline{y}_k = \begin{bmatrix} y_{f,k+1} \\ \underline{y}_{c,k} \\ u_k \end{bmatrix} \tag{66}$$

Equation 66 is modified using the plant dynamics

$$\underline{y}_k = \begin{bmatrix} C_p\Phi_p & 0 & C_p\Gamma_p \\ 0 & I & 0 \\ 0 & 0 & 1 \end{bmatrix} \begin{bmatrix} \underline{x}_p \\ \underline{z} \\ \underline{u} \end{bmatrix}_k + \begin{bmatrix} C_p\Gamma w_k \\ 0 \\ 0 \end{bmatrix} + \underline{\gamma}_k \tag{67}$$

Note that the "measurement noise" and the process noise become cross-correlated. The implementable control law which minimizes the cost function using Eq. 66 as the measurement vector is

$$\underline{z}_k = \Phi_c \, \underline{z}_{k-1} + \Gamma_c \, y_{f,k} + \Gamma_u \, u_{k-1} \tag{68}$$

$$u_k = \Phi_u \, u_{k-1} + K_f \, y_{f,k} + K_c \, \underline{z}_{k-1} \tag{69}$$

A block diagram is shown in Fig. 6. All multiplications and additions in Eq. 69 can be performed before t_k, except the single multiplication $K_f \, y_{f,k}$ and the addition to form u_k. The computation delay is very small. The compensator in the control law in Eq. 68 resembles the "update" Kalman filter form.

The covariance, X_u, for the alternate control structure is reduced to 0.01 to make the control surface variance similiar to the baseline design control surface variance as shown in Table 9. The reduction in X_u degrades the stability properties of the alternate control structure design as shown by the Bode plot in Fig. 7. The performance of the alternate control structure could probably be significantly improved by adjusting the quadratic weights. The quadratic weights are not changed in any of the tests from those used to optimize the baseline design. The low frequency gain in Fig. 7 is unacceptably high, but could be improved using the (s/s+b) washout filter.

VI. EFFECT OF VARYING FLIGHT CONDITION

The active flutter suppression control system should stabilize the wing over a large range of flight conditions. Two approaches are investigated for flutter suppression from $\bar{q}$ = 5.0kPa to 9.5kPa at constant Mach number.

The first approach uses the constant gain baseline design at $\bar{q}$ = 8.0kPas and investigates closed-loop performance with changing flight condition. In the second approach, optimal output feedback designs are obtained at four flight conditions. A new gain scheduling procedure is used to schedule control gains as a function of $\bar{q}$ by minimizing the weighted difference of optimal and gain scheduled closed-loop eigenvalues.

A. CONSTANT GAIN DESIGN

The baseline constant gain design at $\bar{q}$ = 8.0kPas, for the design values shown in Table 4, has the following values for the block diagram shown in Fig. 2,

$$\Phi_c = \begin{bmatrix} 0.746 & 0.0994 & 0.217 & 0.0914 \\ -0.112 & 0.918 & 0.267 & -0.109 \\ 0.139 & -0.274 & 0.256 & -0.227 \\ 0.00942 & 0.0964 & 0.0314 & 0.652 \end{bmatrix} \tag{70}$$

$$\Phi_u = -0.111 \tag{71}$$

$$\Gamma_c = \begin{bmatrix} 0.000155 \\ 0.00216 \\ 0.00336 \\ -0.000343 \\ 0.00947 \end{bmatrix} \tag{72}$$

$$\Gamma_u = \begin{bmatrix} 0.314 \\ 0.231 \\ -0.267 \\ 0.627 \end{bmatrix} \tag{73}$$

$$K_f = 0.00946 \tag{74}$$

$$K_c = \begin{bmatrix} 0.334 & -0.204 & -0.854 & 0.0765 \end{bmatrix} \tag{75}$$

The open-loop wing model eigenvalues for the first seven modes is shown in Fig. 8. The wing model is stable for $\bar{q}$ = 5kPa. The closed-loop wing model eigenvalue root locuses for the constant gain design are shown in Fig. 9, along with the root locus of one of the closed-loop compensator poles. The constant gain design stabilizes the wing up to $\bar{q}$ = 9.5kPa where the closed-loop compensator pole shown goes unstable. Rms response for the control surface, and gain and phase margins are shown in Table 10. The rms response remains at a high level as $\bar{q}$ decreases but the gain and phase margins improve (except for the high frequency phase margin at $\bar{q}$ = 5.0kPas).

B. A NEW GAIN SCHEDULING PROCEDURE

A practical method for adapting a control law to changing flight conditions is gain scheduling. Control designs are obtained at a number of flight conditions which span the operating range of the plant. The gains in the control law are scheduled using regression analysis. Flight condition parameters that can be measured or estimated in flight are treated as independent variables in the regression.

The previous section demonstrated that a constant gain design stabilized the wing over a wide range of dynamic pressure variations. A gain scheduling function of the form

$$K_{gs} = \bar{q}\, G_1 + G_2 \tag{76}$$

should be able to improve both performance and the stability region. A standard regression analysis cost function for computing G_1 and G_2 is

$$J_3 = \sum_{i=1}^{N_f} \text{tr} \left\{ (K_{gs} - K_i) Q_i (K_{gs} - K_i)^T \right\} \tag{77}$$

The gains, K_i, are the optimal output feedback gains obtained at N_f flight conditions. Q_i is a positive definite symmetric weighting matrix, and tr

signifies the trace of a matrix.

The gains G_1 and G_2 were computed using Eq. 77 and Q_i the identity matrix. The closed-loop plant using K_{gs} was unstable within the region of the gain schedule. Adjusting the diagonal elements of Q_i to stabilize the gain-scheduled closed-loop eigenvalues proved to be difficult. An alternative method is developed for choosing Q_i. The new cost function attempts to match closed-loop eigenvalues and eigenvectors instead of matching gain variations.

Consider two feedback gains, K and K_{gs} which have the same dimension but are not equal. The closed-loop eigenvalues, λ_j, and eigenvectors, $\underline{x}_j$, for K satisfy

$$(\Phi + \Gamma K C)\, \underline{x}_j = \lambda_j\, \underline{x}_j \qquad j = 1 \ldots n \tag{78}$$

Following concepts in Ref. 29, assume that K and K_{gs} are related by

$$K C\, \underline{x}_j = K_{gs}\, C\, \underline{x}_j \tag{79}$$

for the eigenvector $\underline{x}_j$. Substituting Eq. 79 into Eq. 78, it follows that K and K_{gs} have the same closed-loop eigenvalue and eigenvector for the plant (Φ, Γ).

The cost function in Eq. 77 is altered using the closed-loop eigenvectors for the known gains, K_i,

$$J_3 = \sum_{i=1}^{N_f} \operatorname{tr} \left\{ (K_{gs} - K_i) \overbrace{(C_i\, X_i\, W_i\, X_i^*\, C_i^T)}^{Q_i} (K_{gs} - K_i)^T \right\} \tag{80}$$

The matrix, X_i, in Eq. 80 is the closed-loop eigenvectors for K_i arranged columnwise. W_i is a diagonal weighting matrix with nonzero positive elements along the diagonal. The notation * means take the transpose of the complex conjugate of the matrix. The matrix Q_i is real if diagonal weights in W_i weight an eigenvector and its complex conjugate equally. The cost function

minimizes the error between $K_{gs}\ C\ \underline{x}_j$ and $K_i\ C\ \underline{x}_j$ instead of between K_{gs} and K_i. Minimizing the cost function yields

$$\begin{bmatrix} G_1 & G_2 \end{bmatrix} \begin{bmatrix} \sum_{i=1}^{N_f} \bar{q}_i^2 Q_i & \sum_{i=1}^{N_f} \bar{q}_i Q_i \\ \sum_{i=1}^{N_f} \bar{q}_i Q_i & \sum_{i=1}^{N_f} Q_i \end{bmatrix} = \begin{bmatrix} \sum_{i=1}^{N_f} \bar{q}_i K_i Q_i \\ \sum_{i=1}^{N_f} K_i Q_i \end{bmatrix} \tag{81}$$

Inverting the square matrix in Eq. 81 determines the least square solution for G_1 and G_2. If a gain scheduled closed-loop eigenvalue is unsatisfactory, the diagonal weight in W_i can be increased in an attempt to force the eigenvalue to its design value. This gain scheduling procedure is particularly applicable to the flutter problem since the primary concern is the stability of one unstable mode.

C. GAIN SCHEDULE DESIGN

The performances for optimal output feedback designs at $\bar{q}$ = 8.0, 7.0, 6.0 and 5.0 kPa are shown in Table 11. The second row in Table 11 shows that rms response can be reduced at lower $\bar{q}$ while maintaining phase and gain margins comparable to $\bar{q}$ = 8.0 kPa. The baseline design and the last three designs in Table 11 are used to compute G_1 and G_2 in Eq. 81.

The scheduled gain performance and closed-loop eigenvalue root-locus are shown in Table 12 and Fig. 10, respectively. Phase and gain margins are high in Table 12 but the resulting rms response is also high. The scheduled gain closed-loop plant goes unstable immediately outside the region of flight conditions used in the gain schedule. The instability is caused by one of the closed-loop compensator poles. New gain scheduling procedures is an area recommended for continued theoretical investigations.

VII. CONCLUSIONS AND RECOMMENDATIONS

A. CONCLUSIONS

The conclusions of this study are

- An efficient stable algorithm for solving the stochastic infinite-time discrete optimal output feedback problem can be applied to active flutter suppression control design.
- Practical discrete low-order dynamic compensators can be designed using optimal output feedback.
- A digital control law which accommodates computation delay can stabilize the wing with reasonable rms performance and adequate, adjustable, gain and phase margins.
- The sampling rate for the control law should be at least 140 samples/sec.
- Lowering the analog prefilter pole increases rms response but also improves one of the gain margins and both phase margins.
- A new gain scheduling procedure is developed to yield a stable linear gain schedule as a function of dynamic pressure over the design flight conditions. Despite these developments, further improvements and modifications in gain scheduling are needed since the gain schedule did not perform as well as a constant gain design inside and outside the design flight conditions.
- Designing the flutter control system using a reduced order model, and verifying performance of the control design with a higher order more exact model, reduced computer cost without significantly compromising control performance.

B. RECOMMENDATIONS

- Further develop the baseline control designs for both structures in Figs. 6 and 2. The goal is to lower control rms response to 4.5 deg and improve the low frequency phase margin. Avenues for further development for the baseline design are
  - Vary the quadratic weights.
  - Increase the prefilter pole to -60.0.
  - Lower the sample rate to 150 samples/sec.
  - Start the algorithm at many different starting gains to determine a lower value for the cost function.
  - Vary the initial condition covariances.
  - Try using a dynamic compensator of order two as in Ref. 11.
  - Introduce a second accelerometer measurement as in Refs. 1 and 28.
  - Move the compensator pole that goes unstable in Fig. 9 further into the left half complex plane.
- Test the active flutter suppression digital control in a wind tunnel.
- Investigate theoretical and numerical developments which may cause the optimal dynamic compensator to be unique (up to a similarity transformation). One avenue is to restrict compensator gains so that the compensator is an observer as discussed in Appendix A. References 9 to 11 did not treat all the control law gains as free parameters.
- Further improve the gain schedule procedure in Section VII-B. Modify the approach so that a select number of gains are scheduled using Eq. 76 and others are chosen to remain constant. Introduce eigenvalue sensitivity into the cost function.

- A potentially better approach to gain scheduling is to bring the selection of G_1 and G_2 in Eq. 76 directly into the control design optimization process. ICS has recently developed a multi-model approach to stochastic optimal output feedback which could perform the optimization.

APPENDIX A

COMPENSATORS AND OBSERVER THEORY

The globally optimal output feedback constrained dynamic compensator solution is currently unresolved if the order of the compensator is prespecified to be less than n-ℓ. If the order is increased to n-ℓ, where ℓ is the number of observations, then Ref. 7 shows the globally optimum dynamic compensator is an observer which estimates the n-ℓ state functional not measured with the ℓ measurements. If the order is increased to n, the optimal solution uses a Kalman filter for the compensator. These results suggest the optimal compensator which minimizes stochastic performance may be some type of observer of a linear function of plant states not measured. The cross weighting used in Eq. 26 is a straightforward attempt to cause this behavior to occur. This appendix addresses three questions about compensators that resulted from the cross-weighting approach:

- When is a compensator an observer of a linear function of plant states?
- If the compensator is an observer, what does it observe?
- When are two internal compensator representations related by a state transformation and what is the transformation matrix?

These questions are resolved using the theory of feedforward control developed in Ref. 30. Given a plant

$$\underline{z}_{k+1} = \Phi_c \underline{z}_k + \Gamma_c \underline{u}_{c,k} \tag{82}$$

$$\underline{y}_{c,k} = K_c \underline{z}_k + K_f \underline{u}_{c,k} \tag{83}$$

and a model

$$\underline{x}_{k+1} = \Phi \underline{x}_k + \Gamma \underline{u}_{,k} \tag{84}$$

$$\underline{y}_k = H\underline{x}_k + D\underline{u}_k \quad , \quad \underline{y}_{obs,k} = C\underline{x}_k \tag{85a,b}$$

the plant trajectory, $\underline{z}^*_k$ and control, $\underline{u}^*_{c,k}$ which causes $\underline{y}_{c,k}$ to follow $\underline{y}_k$ is

$$\begin{bmatrix} \underline{z}^*_k \\ \underline{u}^*_{c,k} \end{bmatrix} = \begin{bmatrix} S_{11} & S_{12} & S_{13}..... \\ S_{21} & S_{22} & S_{23}..... \end{bmatrix} \begin{bmatrix} \underline{x}_k \\ \underline{u}_k \\ \underline{u}_{k+1} \\ . \\ . \\ . \end{bmatrix} \tag{86}$$

The feedforward matrices in Eq. 86, if they exist, satisfy the algebraic equation

$$\begin{bmatrix} \Phi_c & \Gamma_c \\ K_c & K_f \end{bmatrix} \begin{bmatrix} S_{11} & S_{12} & S_{13} \cdots \\ S_{21} & S_{22} & S_{23} \cdots \end{bmatrix} = \begin{bmatrix} S_{11}\Phi & S_{11}\Gamma & S_{12} \cdots \\ H & D & 0 \cdots \end{bmatrix} \tag{87}$$

If S_{12} is a zero matrix, then S_{1j} and S_{2j}, $j \geq 3$ are also all zero matrices. The normal use of Eq. 86 is that the plant and model are given and it is desired to find $\underline{z}^*$ and $\underline{u}^*_c$.

An observer is a form of model following. In an observer, it is desired to choose Φ_c stable, Γ_c, K_c, K_f and Γ_u so that $\underline{y}_c = y$ without using future values of $\underline{u}$ and using only $\underline{y}_{obs}$ in $\underline{u}^*_c$. With these restrictions, Eq. 87 changes to

$$\begin{bmatrix} \Phi_c & \Gamma_c \\ K_c & K_f \end{bmatrix} \begin{bmatrix} S_{11} & 0 & 0 \ldots \\ C & S_{22} & 0 \ldots \end{bmatrix} = \begin{bmatrix} S_{11}\Phi & S_{11}\Gamma & 0 \ldots \\ H & D & 0 \ldots \end{bmatrix} \tag{88}$$

If the equations in Eq. 88 are individually expanded, the standard observer conditions are obtained.

$$\Phi_c S_{11} + \Gamma_c C = S_{11}\Phi \tag{89}$$

$$\Gamma_u = \Gamma_c S_{22} = S_{11}\Gamma \tag{90}$$

$$K_c S_{11} + K_f C = H \tag{91}$$

$$K_f S_{22} = D \tag{92}$$

If $\underline{u}_c^*$ is applied to Eq. 82, the plant equations become

$$\underline{z}_{k+1} = \Phi_c \underline{z}_k + \Gamma_c \underline{y}_{obs,k} + \Gamma_u \underline{u}_k \tag{93}$$

$$\underline{y}_{c,k} = K_c \underline{z}_k + K_f \underline{y}_{obs,k} + D\underline{u}_k \tag{94}$$

and $\underline{y}_c$ observes $\underline{y}$.

Comparing Eq. 93 with Eq. 38, the answer to the first question is that the compensator is an observer if the compensator matrices satisfy Eqs. 89 to 92. The answer to the second question is that the compensator/observer state, $\underline{z}_k$, observes $S_{11}\underline{x}_k$.

Equations 89 to 92 imply that if the compensator is to be an observer, then the gains in Eq. 93 cannot all be treated as free parameters. For example, if K_Φ and K_y in Eq. 38 are specified, then S_{11} in Eq. 89 can be computed and K_u is forced to become

$$K_u = \frac{1}{\Delta t} S_{11}\Gamma \tag{95}$$

Equality constraints, such as Eq. 95, could be used to change the cost function in Eq. 48.

The answer to the third question can be determined if one compensator is treated as the plant and the other compensator is treated as a model so that the feedforward matrix equation can be solved. If equality holds in Eq. 87, S_{12} and S_{21} are zero matrices and S_{22} is an identity matrix, then the compensators are alternate internal representations of the same input-output relationship. The compensator states are then related by the linear transformation S_{11}.

REFERENCES

1. Mahesh, J.K., Garrard, W. G., Stone, C. R., and Hausman, P. D., Active Flutter Control for Flexible Vehicles, Volume 1 - Final Report. NASA CR-159160, 1979.

2. Newsome, Jerry R., A Method for Obtaining Practical Flutter-Suppression Control Laws Using Results of Optimal Control Theory, NASA TP-1471, 1979.

3. Gangsaas, Dagfinn, and Ly, Uy-loi, "Application of a Modified Linear Quadratic Gaussian Design to Active Control of a Transport Airplane", AIAA Paper 79-1746, Aug. 1979.

4. Levine, W. S., Johnson, T. L., and Athans, M., "Optimal Limited State Variable Feedback Controllers for Linear Systems", IEEE Trans. Automatic Control, Vol. AC-16, Dec. 1971, pp. 785-793.

5. Mendel, J. M., and Feather, J., "On the Design of Optimal Time-Invariant Compensators for Linear Stochastic Time-Invariant Systems," IEEE Trans. Automatic Control, Vol. 20, Oct. 1975, pp. 653-656.

6. Kurtaran, B., "Suboptimal Control for Discrete Linear Constant Stochastic Systems," IEEE Trans. Automatic Control, Vol. AC-20, June 1975, pp. 423-425.

7. Blanvillain, P. J. and Johnson, T. L., "Invariants of Optimal Minimal-Order Observer Based Compensators, "IEEE Trans. Automatic Control, Vol. AC-23, June 1978, pp. 473-474.

8. Halyo, N. and Broussard, J. R., "A Convergent Algorithm for the Stochastic Infinite-Time Discrete Optimal Output Feedback Problem", Proceedings of the 1981 JACC, Charlottesville, Va., June 1981.

9. Martin, G. D. and Bryson, A. E., "Attitude Control of a Flexiable Spacecraft", Vol. 3, January-February, 1980, pp. 37-41.

10. Mukhopadhyay, V., Newsom, J. R. and Abel, I., "A Method for Obtaining Reduced-Order Control Laws for High-Order Systems Using Optimization Techniques", NASA TP-1876, August 1981.

11. Karpel, M., "Design for Active and Passive Flutter Suppression and Gust Alleviation, NASA CR-3482, November 1981.

12. Srinivasa, Y. G. and Rajagopalan, T., "Algorithms for the Computation of Optimal Output Feedback Gains", Proc. of 18th IEEE Conference on Decision and Control, Fort Lauderdale, Florida, December 1979.

13. Safonov, M. G. and Athans, M., "Gain and Phase Margin for Multiloop LQG Regulators", IEEE Trans. Automatic Control, IEEE Trans. Automatic Control Vol. AC-22, April 1977, pp. 173-179.

14. Doyle, J. C. and Stein, G., "Robustness with Observers", IEEE Trans. Automatic Control, Vol. AC-24, August 1979, pp. 607-611.

15. Pines, S. and McConnell, J., "An Influence Coefficient Method for the Application of the Modal Technique to Wing Flutter Suppression of the DAST ARW-1- Wing, AMA Report No. 81-25, July 1981.

16. Abel, I., An An Analytic Technique for Predicting the Characteristics of a Flexible Wing Equipped with an Acive Flutter Suppression System and Compared with Wind Tunnel Data, NASA TN-1367, 1979.

17. Nissim, E., and Abel, I., Development and Application of an Optimization Procedure for Flutter Suppression Using the Aerodynamic Energy Concept, NASA TP-1137, February, 1978.

18. Edwards, J. W., Breakwell, J. V., and Bryson, A. E., "Active Flutter Control Using Generalized Unsteady Aerodynamic Theory," Journal Guidance and Control, Volume 1, January - February, 1978.

19. Franklin, G. F., and Powell, J. D., Digital Control of Dynamic Systems, Addison-Wesley Publishing Company, Rading. Mass, 1981.

20. Smith, C. L., Digital Computer Process Control, Intext Educational Publishers, Scranton, Penn., 1972.

21. Broussard, J. R., Berry, P. W. and Stengel, R. F., "Modern Digital Flight Control Systems Design for VTOL Aircraft", NASA CR-159019, March 1979.

22. Mahesh, J. K. and Konar, A. F., "Interactive Flight Control System Analysis Program," NASA NAS1-16438, November 1981.

23. Moore, B. C., "Principal Component Analysis in Linear Systems: Controllability, Observability, and Model Reduction", IEEE Trans. Automatic Control, Vol. AC-26, February 1981, pp. 17-32.

24. Tyler, J. S., Jr., "The Characteristics of Model Following Systems as Synthesized by Optimal Control," IEEE Transactions on Automatic Control, Vol. AC-9, October 1964, pp. 485-498.

25. Kreindler, E. and Rothschild, "Model-Following in Linear-Quadratic Optimization," AIAA Journal 14, 7, pp. 835-842, July 1976.

26. Halyo, N. and Caglayan, A. K., "A Separation Theorem for the Stochastic Sampled-Data LQG Problem," International Journal of Control, Vol. 23, Feb. 1976, pp. 237-244.

27. Armstrong, E. S., ORACLS - A Design System for Linear Multivariable Control, Marcel-Dekher, Inc., New York, 1980.

28. Noll, T. E., Huttsell, L. J. and Cooley, D. E., "Wing/Store Flutter Suppression Investigation", Journal of Aircraft, Vol. 18, November 1982, pp. 969-975.

29. Broussard, J. R., "A Quadratic Weight Selection Algorithm," Proceedings of the 1981 JACC, Charlottesville, VA., June 1981.

30. Broussard, J. R., and O'Brien, M. J., "Feedforward Control to Track the Output of a Forced Model", IEEE Trans. Automatic Control, Vol. 25, August 1980, pp. 851-854.

LIST OF SYMBOLS

In general, matrices are represented by capital letters and vectors are underscored.

VARIABLE	EQUATION	DESCRIPTION
A	23	Reduced-order design wing model system matrix
A_a	23	Fast actuator model pole
A_g	23	Reduced-order disturbance pole
$\bar{A}_{ii}$	19	Partitioned, transformed wing model system matrix
A_w	6	52 x 52 wing model system matrix
a	12	Prefilter pole
a_i	18	Real part of an eigenvalue
B	23	Reduced-order design wing model control matrix
B_a	23	Control matrix for fast actuator model
B_g	23	Control matrix for reduced-order disturbance model
B_u	6	52 x 1 wing model control matrix
$\bar{B}_{ui}$	19	Partitioned, transformed wing model control matrix
B_w	6	52 x 1 wing model disturbance noise matrix
$\bar{B}_{wi}$	19	Partitioned, transformed wing model disturbance noise matrix
b_1	18	Imaginary part of an eigenvalue

VARIABLE	EQUATION	DESCRIPTION
C	2, 28	Observation matrix
C_p	24	Reduced-order plant state observation matrix
C_w	7	1 x 52 wing model state observation matrix
$\bar{C}_{wi}$	20	Partitioned, transformed wing model state observation matrix
$\bar{D}$	22	$D_w - \bar{C}_{w2}\ \bar{A}_{22}^{-1}\ \bar{B}_{u2}$
D_w	7	Wing model control observation matrix
$d(K_i)$	58	Difference between gains
E	23	Disturbance observation matrix
$\bar{E}$	22	$E_w - \bar{C}_{w2}\ \bar{A}_{22}^{-1}\ \bar{B}_{w2}$
E_w	7	External disturbance observation matrix
F	55	Positive definite symmetric matrix
G	56	Positive definite symmetric matrix
G_i	76	Gain schedule gain
H_c	26	Cross-weighting observation matrix
h_i	8	Vertical deflection at node i
I	3	Identity matrix
J, J_t	30, 42	
J_s, J_3	43, 77	Cost Function
j	17b	$\sqrt{-1}$
K	1	Gain matrix
$\bar{K}_c$, K_c	36, 37	Gain matrix from compensator state to plant control rate
$\bar{K}_f$, K_f	31, 36	Gain from prefilter observation to plant control rate
K_{gs}	76	Gain scheduled gain matrix
K_{NEW}	57	Projected direction of optimal gain in algorithm
K_u	31	Gain matrix from plant control to compensator control

VARIABLE	EQUATION	DESCRIPTION
K_v	31	Gain from plant control to plant control rate
K_y	31	Gain matrix from prefilter observation to compensator control
K_Φ	31	Gain matrix from compensator state to compensator control
k	1	Index integer
L	9	Scale of turbulence
ℓ	-	Number of measurements
$\hat{M}$	29	Discrete cost function state, control cross-weighting matrix
N	29	Number of time steps in cost function
N_f	77	Number of design flight conditions
n	-	Number of states
P	49	Solution matrix to cost equation
$\hat{P}$	55	Intermediate algorithm computation
Q	5	Cross-weighting matrix between plant and compensator
$\hat{Q}$	29	Discrete cost function state weighting matrix
Q_c	25	Weighting matrix for compensator states
Q_i	77	Weighting matrix for gain schedule
Q_l	25	Weighting matrix for wing model states
$\bar{q}$	-	Dynamic pressure
R	25	Weighting matrix for wing model control
$\hat{R}$	29	Discrete cost function control weighting matrix
R_c	25	Weighting matrix for compensator controls
R_v	25	Weighting matrix for wing model control rate
s	9	Laplace transform variable
S_{ij}	86	Feedforward matrix

VARIABLE	EQUATION	DESCRIPTION
S	51	Solution matrix to covariance like equation
$\hat{S}$	56	Intermediate algorithm computation
T	17a	Block diagonalizing transformation matrix
t	-	Time
u	1	Control State
u_c	3	Compensator control state
V	45b	Measurement noise covariance
V_f	9	Aircraft velocity
v	13	Control rate
W	44b	Plant process noise covariance
W_1	80	Diagonal weighting matrix in gain schedule
$\underline{w}$	27	Discrete plant process noise
S_o	47	Initial condition covariance
X_u	-	Control actuator state initial condition covariance matrix
$\underline{x}$	27	State vector
x_a	8	Actuator state
$\underline{x}_d$	8	Disturbance state vector
$\underline{x}_g$	8	Dryden wind model state vector
$\bar{\underline{x}}_g$	23	Reduced and balanced disturbance/gust state vector
$\underline{x}_i$	80	Complex eigenvector
$\underline{x}_p$	23	Plant state vector for reduced model
$\underline{x}_{qa}$	8	Unsteady lift and moment state vector
$\underline{x}_w$	6	52 x 1 wing model state vector
$\bar{\underline{x}}_{w1}$, $\bar{\underline{x}}_{w2}$	19, 20	Partitioned, transformed wing model state vectors

VARIABLE	EQUATION	DESCRIPTION
y_{obs}, y	85b, 2	Measurement vector
$\underline{y}_c$	4	Compensator state measurement vector
y_f	12	Prefilter state measurement
$\underline{z}$	3	Compensator state vector

VARIABLE (GREEK)	EQUATION	DESCRIPTION
α_i	59	Algorithm stability parameter
β	13	Continuous model compensator stability parameter
β_1, β_2	3	Discrete model compensator stability parameter
Γ	27	Plant discrete control matrix
Γ_c	82	Compensator control matrix
Γ_p	27	Wing model discrete control matrix
Γ_u	35	Control discrete control matrix
Γ_w	27	Wing model discrete disturbance matrix
γ	2	Measurement noise
γ_a	7	Accelerometer Measurement Noise
δ_a	8	Actuator position
δ_h	6	Actuator housing white noise disturbance state
λ	16	Complex eigenvalue
ξ_g	9	Gust state vector
Σ	29	Summation
σ	-	Number of compensator states
σ_{wg}	9	Variance of gust
ε	53	Small number greater than zero

VARIABLE (GREEK)	EQUATION	DESCRIPTION
Φ	27	Plant state transition matrix
Φ_c	82	Compensator state transition matrix
Φ_{CL}	50	Closed-loop plant matrix
Φ_p	27	Wing model state transition matrix
Φ_u	33	Control state transition matrix
Δt	-	Control and measurement sample interval

SPECIAL OPERATORS	DESCRIPTION
$(\dot{})$	Derivative of quantity with respect to time
$(\underline{\ })$	Vector quantity
$\partial(\ )/\partial(\ )$	Partial derivative of one variable with respect to another
$(\ )^*$	Complex conjugate transpose
$(\ )^*$	Star trajectory
∞	Infinity
$\int$	Integral
$E[\ ]$	Expected Value
$(\ )^T$	Transpose
$(\ )^{-1}$	Inverse

ACRONYM	CORRESSPONDING PHRASE
LQG	Linear quadratic Gaussian
LQR	Linear quadratic regulator
tr	Trace of a square matrix

TABLE 1 POLES AND ZEROES OF THE WING MODEL

	OPEN-LOOP EVALUATION MODEL POLES	EVALUATION MODEL ZEROES
MODES USED FOR BODE PLOT	10.8 ± j59.8	13.9
	-40.0 ± j78.5	-50.0
	-5.8 ± j162.3	-4.2 ± j163.0 *
	-40.0 ± j225.5	-39.4 ± j226.9 *
	-125.0 ± j352.3	-228.0 ± j1019.0
	-26.4 ± j377.3	-21.9 ± j370.0
	-16.5 ± j418.2	-5.1 ± j415.2
	-37.4 ± j557.0	-19.0 ± j545.0
MODES THAT FOLD FOR $\Delta t = 0.005$	-36.6 ± j663.0	-36.3 ± j659.0 *
	-34.6 ± j776.0	-4.4 ± j770.0
	-39.7 ± j820.0	-54.7 ± j812.0
	-59.0 ± j908.0	-59.0 ± j906.0 *
	-16.0 ± j1278.0	-89.7 ± j1338.0
	-17.7 ± j1862.0	-32.6 ± j1891.0
	-20.8 ± j2638.0	-21.2 ± j2639.0 *
	-28.4 ± j5617.0	0.0 ± j0.0
MODES RESIDUALIZED AND NOT USED IN REDUCED MODEL DESIGN	-228.0	-228.0 *
	-232.0	-232.0 *
	-254.0	-254.0 *
	-266.0	-265.0 *
	-284.0	-284.0 *
	-294.0	-294.0 *
	-320.0	-321.0 *
	-332.0	-332.0 *
	-364.0	-369.0 *
	-379.0	-381.0 *
	-421.0	-482.0
	-426.5	-425.0 *
	-501.7 ± j2.3	-497.0
	-706.0	-714.0 ± j34.9

* The pole and zero almost cancel for the actuator to accelerometer output wing model transfer function.

TABLE 2 CONTROL PERFORMANCE FOR ANALOG DESIGNS

REFERENCE	RMS RESPONSE		GAIN MARGIN				PHASE MARGIN			BANDWIDTH @ - 6 dB
	δ_{rms} deg	$\dot{\delta}_{rms}$ deg/sec	dB	rad/sec	dB	rad/sec	deg	rad/sec	deg	rad/sec
Ref. 1, $\bar{q}$ = 7.66 kPa	3.16	180.3	5.5	64	5.0	149	-65.5	51	39.6	101
Ref. 10, $\bar{q}$ = 7.66 kPa	5.2	230.4	5.0	60	12.3	314	-46.0	47	53.0	83

TABLE 3 OPEN AND MAPPED CLOSED-LOOP POLE LOCATIONS

	OPEN-LOOP EVALUATION MODEL POLES	MAPPED CLOSED-LOOP EVALUATION WING MODEL POLES	MAPPED CLOSED-LOOP REDUCED-ORDER WING MODEL POLES
MODES USED IN REDUCED MODEL DESIGN	10.8 ± j59.8	-14.8 ± j59.7	-15.5 ± j59.7
	-40.0 ± j78.5	-76.8 ± j139.0	-79.2 ± j143.0
	-5.8 ± j162.3	-6.8 ± j161.0	-6.9 ± j161.0
	-40.0 ± j225.5	-41.0 ± j225.0	-41.0 ± j225.0
	-125.0 ± j352.3	-149.0 ± j442.0	-136.0 ± j435.0
MODES USED FOR BODE PLOT	-26.4 ± j337.3	-26.0 ± j375.0	
	-16.5 ± j418.2	-15.4 ± j416.0	
	-37.4 ± j557.0	-38.8 ± j558.0	
MODES THAT FOLD FOR $\Delta t = 0.005$	-36.6 ± j663.0	-36.4 ± j593.0	
	-34.6 ± j776.0	-34.6 ± j480.0	
	-39.7 ± j820.0	-39.7 ± j436.0	
	-59.0 ± j908.0	-59.0 ± j348.0	
	-16.0 ± j1278.0	-15.7 ± j21.8	
	-17.7 ± j1862.0	-17.7 ± j606.0	
	-20.8 ± j2638.0	-20.8 ± j125.0	
	-28.4 ± j5617.0	-28.4 ± j591.0	
	-228.0	-228.0	
	-232.0	-232.0	
	-254.0	-254.0	
	-266.0	-266.0	
	-284.0	-284.0	
	-294.0	-294.0	
	-320.0	-321.0	
	-332.0	-332.0	
	-364.0	-348.0	
	-379.0	-381.0	
	-421.0	-538.0	
	-426.5	-425.0	
	-501.7 ± j2.3	-497.0, -485.0	
	-706.0	-725.0	

TABLE 4 NONZERO DIAGONAL ELEMENT DESIGN PARAMETERS

		WEIGHT	COVARIANCE
Wing Mode 1	$- Q_1$	$(2.24)^2$	
Wing Mode 1	$- X_o$		$(3.16)^2$
4 Compensator States	$- Q_c$	$(0.316)^2 I$	
4 Compensator States	$- X_o$		$(10.0^2) I$
Actuator Control Position	$- R$	$(1.0)^2$	
Compensator Control Position	$- R_c$	$(1.0)^2 I$	
Actuator Control Rate	$- R_v$	$(1.23)^2$	
Actuator Control Position	$- X_u$		TABLES 5,7, 8,9,10,11,12
Accelerometer Measurement Noise	$- V_a$		$(0.1)^2$
Cross Coupling Weight	$- Q$	$(31.6)^2$	

TABLE 5 EFFECT OF VARYING INPUT NOISE COVARIANCE

INPUT NOISE COVARIANCE	EVALUATION MODEL RMS RESPONSE				GAIN MARGIN REDUCED MODEL				PHASE MARGIN REDUCED MODEL				BANDWIDTH. @ - 6dB
X_u	u_{rms}, deg	v_{rms}, deg/sec	δ_{rms}, deg	$\dot{\delta}_{rms}$, deg/sec	dB	rad/sec	dB	rad/sec	deg	rad/sec	deg	rad/sec	rad/sec
0.0	7.0	380	4.2	233	2.4	61	-4.2	98	-13.3	51	28.4	78	107
0.1	10.0	392	5.8	227	5.0	60	-7.5	156	-27.5	46	50.6	81	135
1.0	11.4	392	6.6	227	5.6	60	-8.0	190	-34.0	45	55.0	81	154

TABLE 6 VARIANCE OF NODE DEFLECTIONS WITH 0.3048 m/s WIND GUST FOR THE NOMINAL CONTROL DESIGN

NODE POSITION (CENTIMETERS)						
1	2	3	4	5	6	7
0.013	0.10	0.25	0.47	0.74	1.1	1.4
NODE ROTATION (DEG)						
1	2	3	4	5	6	7
0.02	0.08	0.13	0.19	0.27	0.38	0.48

TABLE 7 EFFECT OF LOWERING SAMPLE RATE

STARTING GAIN DIFFERENT	SAMPLES PER SECOND	INPUT NOISE COVARIANCE	EVALUATION MODEL RMS RESPONSE		GAIN MARGIN, REDUCED MODEL				PHASE MARGIN, REDUCED MODEL				BANDWIDTH @ - 6dB
	$1.0/\Delta t$	X_u	δ_{rms}, deg	$\dot{\delta}_{rms}$, deg/sec	dB	rad/sec	dB	rad/sec	deg	rad/sec	deg	rad/sec	rad/sec
NO	200	0.1	5.8	227	5.0	60	-7.5	156	-27.5	45	50.6	81	142
NO	160	0.25	5.9	219	5.1	60	-6.3	155	-30.5	46	48.5	80	151
YES	140	0.25	5.5	210	5.0	60	-6.0	152	-30.2	47	45.0	80	148
YES	100	0.25	5.1	171	4.4	60	-5.5	138	-29.0	48	37.0	78	NONE

TABLE 8 EFFECT OF PREFILTER POLE VARIATION

STARTING GAIN DIFFERENT	PREFILTER POLE, a, sec^{-1}	INPUT NOISE COVARIANCE X_u	EVALUATION MODEL RMS RESPONSE		GAIN MARGIN REDUCED MODEL				PHASE MARGIN, REDUCED MODEL				BANDWIDTH @ - 6dB
			δ_{rms}, deg	$\dot{\delta}_{rms}$, deg/sec	dB	rad/sec	dB	rad/sec	deg	rad/sec	deg	rad/sec	rad/sec
NO	-60.0	0.1	5.4	222	4.7	59	-8.2	149	-26.0	46	45.6	79	120
NO	-50.0	0.1	5.8	227	5.0	60	-7.5	156	-27.5	45	50.6	81	142
NO	-40.0	0.1	5.9	226	5.1	58	-7.3	156	-28.0	45	51.9	81	143
YES	-30.0	0.1	6.1	225	5.4	58	-7.1	157	-30.0	46	52.1	82	144

TABLE 9 EFFECT OF DIFFERENT CONTROL STRUCTURE

STARTING GAIN DIFFERENT	CONTROL STRUCTURE	INPUT NOISE COVARIANCE	EVALUATION MODEL RMS RESPONSE		GAIN MARGIN, REDUCED MODEL				PHASE MARGIN, REDUCED MODEL				BANDWIDTH @ - 6dB
		X_u	δ_{rms}, deg	$\dot{\delta}_{rms}$, deg/sec	dB	rad/sec	dB	rad/sec	deg	rad/sec	deg	rad/sec	rad/sec
NO	FIG. 2	0.1	5.8	227	5.0	60	-7.5	156	-27.5	45	50.6	81	142
NO	FIG. 6	0.01	5.6	228	5.0	57	-7.8	136	-24.5	46	44	87	120

TABLE 10 CONSTANT GAIN DESIGN WITH VARYING DYNAMIC PRESSURE

DYNAMIC PRESSURE $\bar{q}$, kPa	INPUT NOISE COVARIANCE X_u	EVALUATION MODEL RMS RESPONSE		GAIN MARGIN, REDUCED MODEL				PHASE MARGIN, REDUCED MODEL				BANDWIDTH @ - 6 dB
		δ_{rms}, deg	$\dot{\delta}_{rms}$, deg/sec	dB	rad/sec	dB	rad/sec	deg	rad/sec	deg	rad/sec	rad/sec
9		9.9	340				NOT	DETERMINED				
8.5		7.0	257									
8	0.1	5.8	227	5.0	60	-7.5	156	-27.5	45	50.6	81	142
7		4.8	207	6.4	57	-8.0	155	-42	50	71	77	129
6		4.4	206	9.8	54	-8.5	153	-120	48	74	60	120
5		4.4	216	---	---	-9.6	152	-158	32	20	54	57

TABLE 11 OPTIMAL OUTPUT FEEDBACK DESIGNS FOR VARYING DYNAMIC PRESSURES

STARTING GAIN DIFFERENT	DYNAMIC PRESSURE $\bar{q}$, kPa	INPUT NOISE COVARIANCE X_u	EVALUATION MODEL RMS RESPONSE		GAIN MARGIN, REDUCED MODEL				PHASE MARGIN, REDUCED MODEL				BANDWIDTH @ - 6 dB
			δ_{rms}, deg	$\dot{\delta}_{rms}$, deg/sec	dB	rad/sec	dB	rad/sec	deg	rad/sec	deg	rad/sec	rad/sec
NO	8	0.1	5.8	227	5.0	60	-7.5	156	-27.5	45	50.6	81	142
NO	7	0.005	4.3	223	4.3	57	-7.5	105	-30	52	52	70	97
NO	7	0.25	5.8	246	7.9	53	-9.1	200	-58	49	86	56	151
NO	6	0.25	4.3	214	7.2	56	-8.0	190	-44	47	80	73	158
NO	5	0.25	1.8	83	---	---	-9.3	204	-67	45	135	50	155

TABLE 12 SCHEDULED GAIN DESIGN WITH VARYING DYNAMIC PRESSURE

DYNAMIC PRESSURE $\bar{q}$, kPa	INPUT NOISE COVARIANCE X_u	EVALUATION MODEL RMS RESPONSE		GAIN MARGIN, REDUCED MODEL				PHASE MARGIN, REDUCED MODEL				BANDWIDTH @ - 6 dB
		δ_{rms}, deg	$\dot{\delta}_{rms}$, deg/sec	dB	rad/sec	dB	rad/sec	deg	rad/sec	deg	rad/sec	rad/sec
8.0	0.1	5.4	211	5.6	60	-5.5	133	-32	46	42	85	142
7.0		5.9	274	4.6	55	-6.3	145	-26	49	91	76	142
6.0		5.8	285	8.3	51	-7.1	148	-30	48	125	58	138
5.0		NOT DETERMINED		---	---	-8.0	149	-60	45	141	53	135

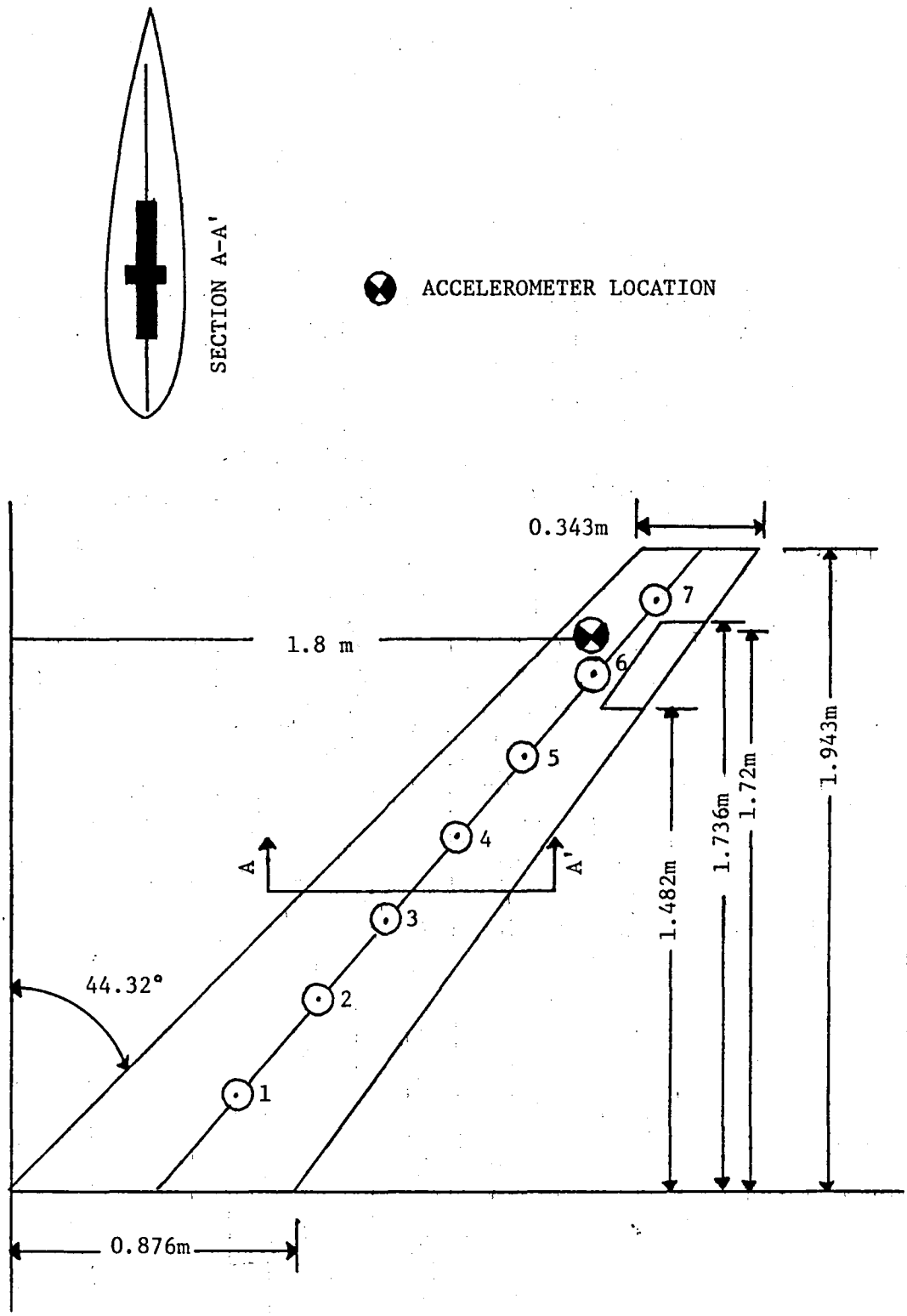

FIGURE 1 WING GEOMETRY, SENSOR AND CONTROL SURFACE LOCATION

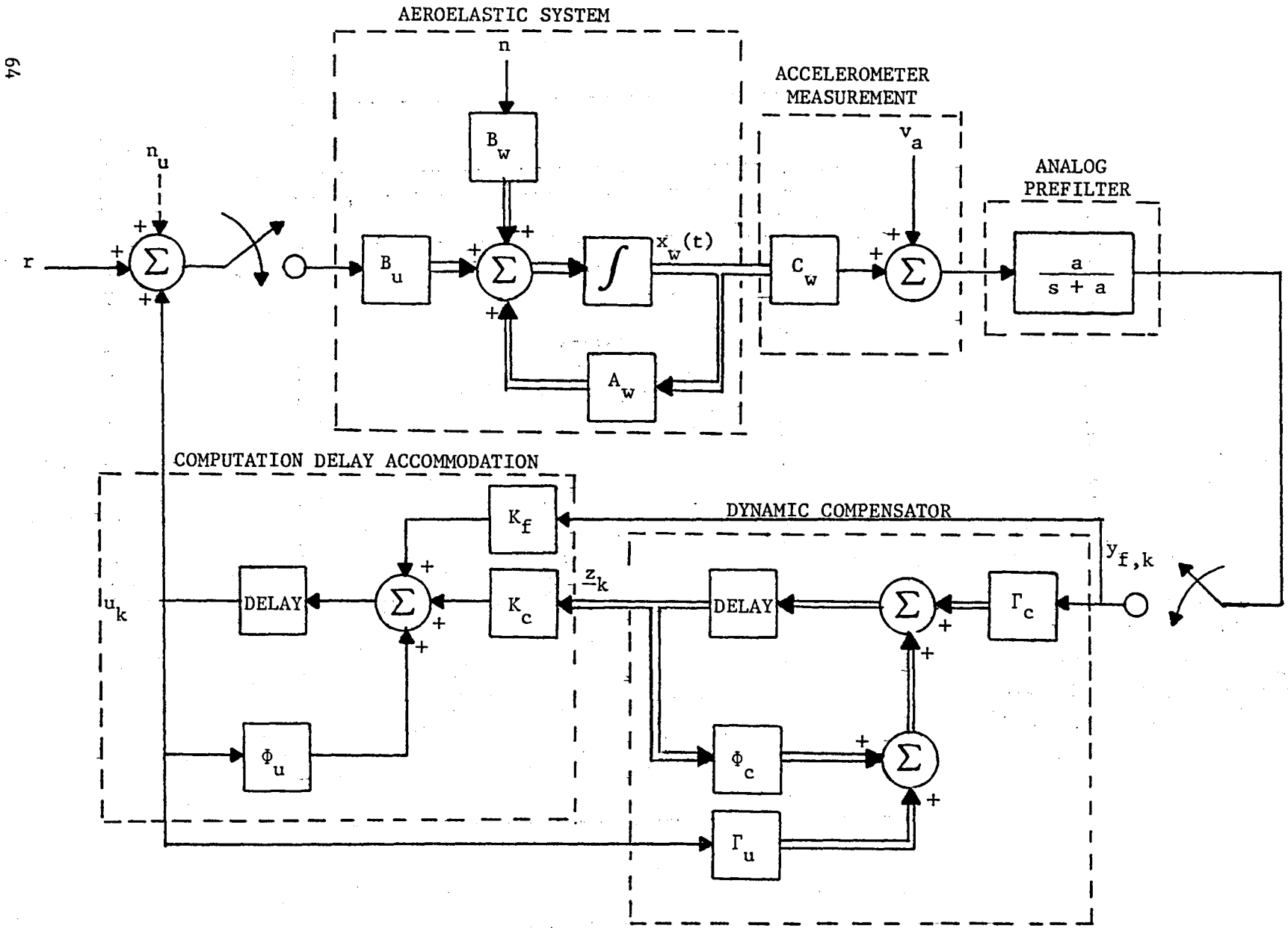

FIGURE 2 CONTROL LAW BLOCK DIAGRAM

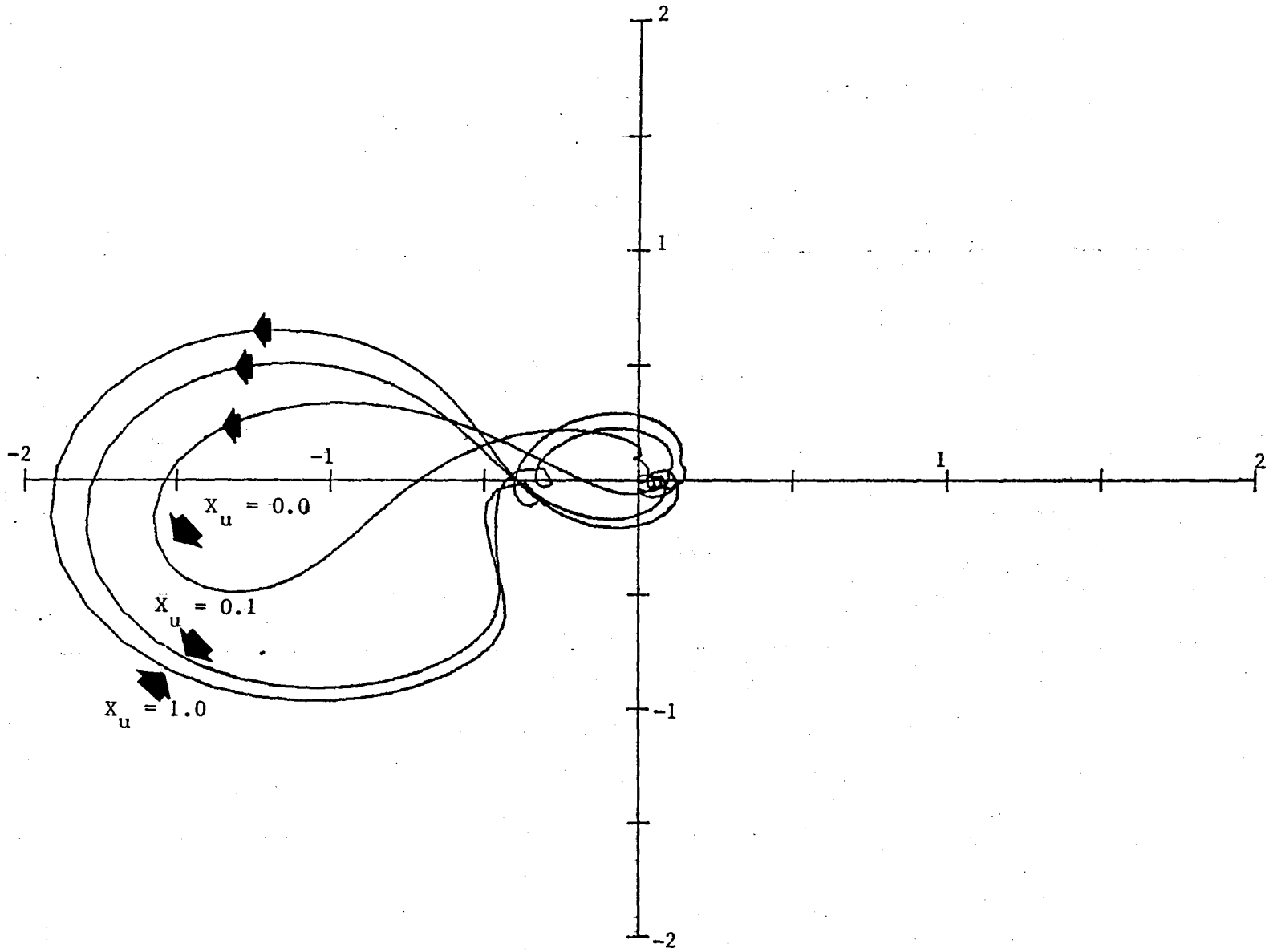

FIGURE 3 NYQUIST DIAGRAMS FOR CONTROL DESIGNS

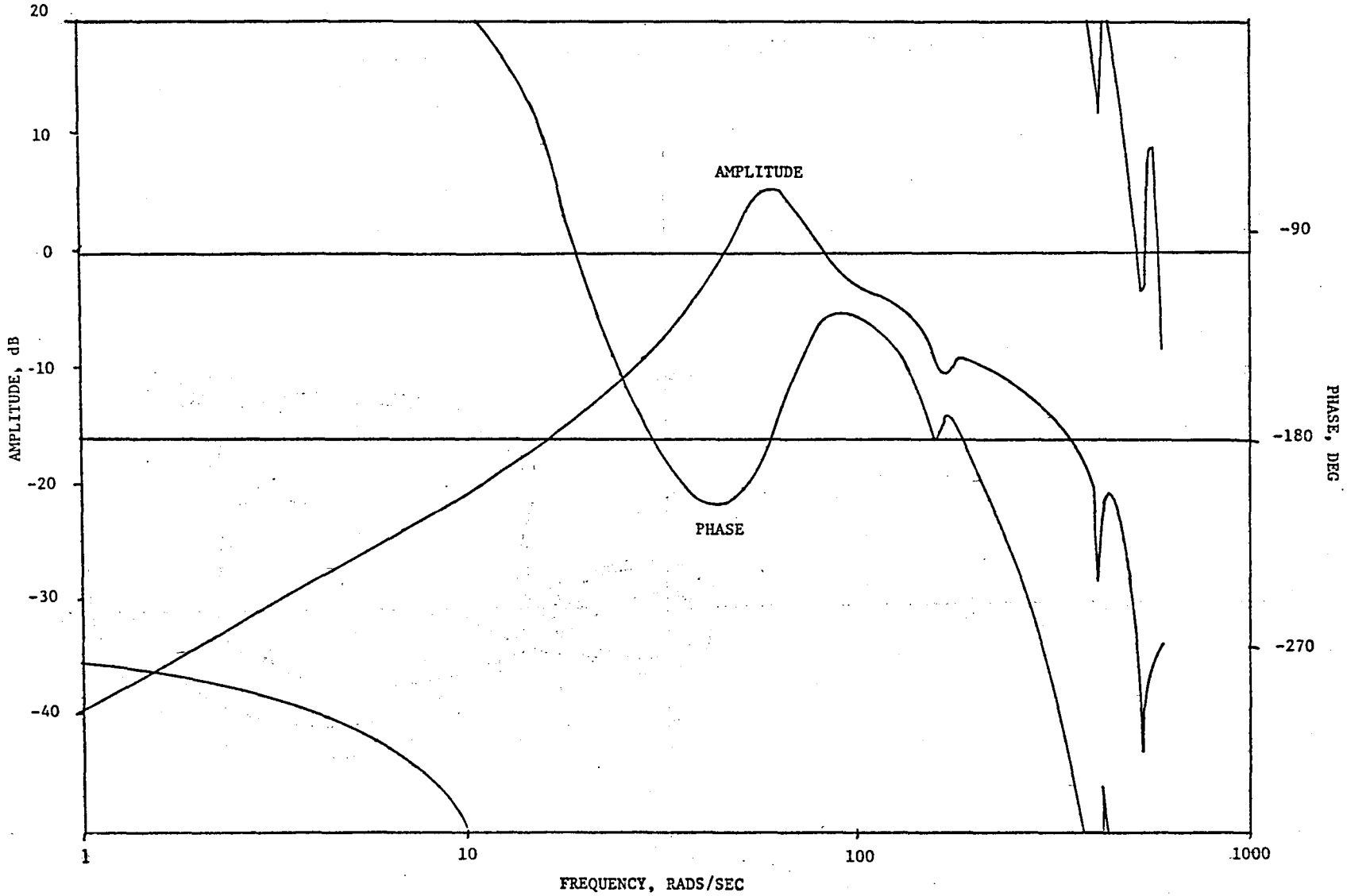

FIGURE 4 BODE PLOT OF REDUCED ORDER EVALUATION MODEL AND DIGITAL CONTROL LAW USING $X_u = 1.0$ AT A DYNAMIC PRESSURE OF 8.0 kPa

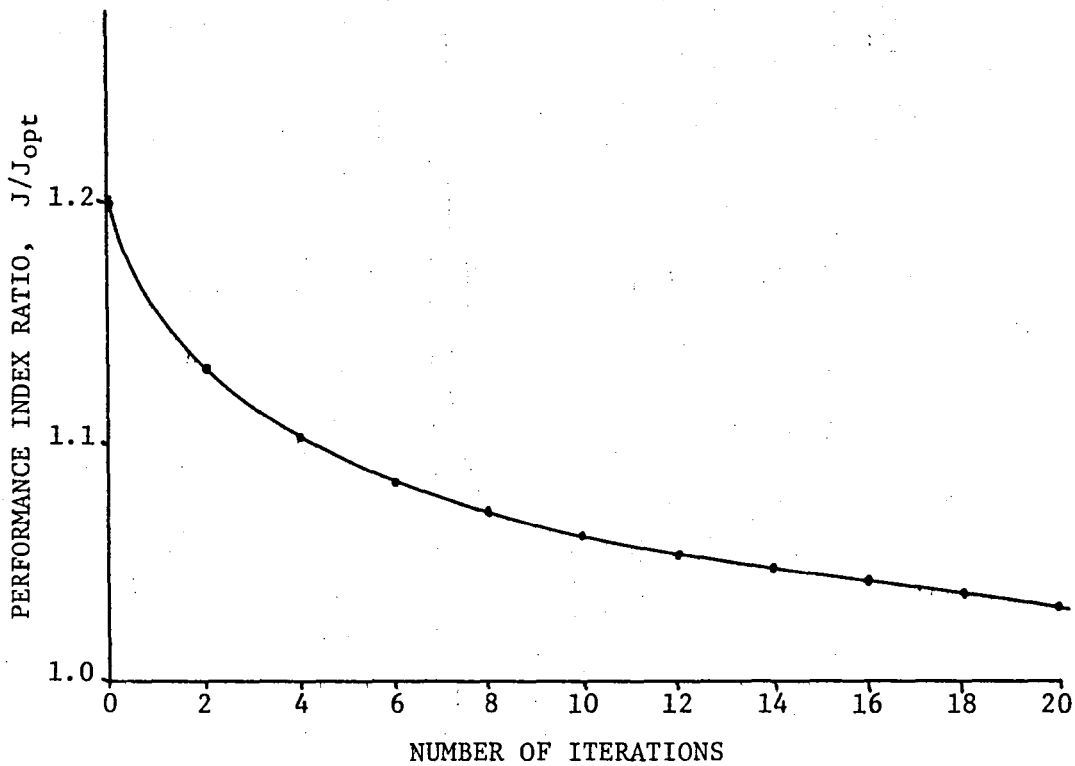

FIGURE 5 TYPICAL CONVERGENCE PATTERN OF PERFORMANCE INDEX USING OUTPUT FEEDBACK ALGORITHM

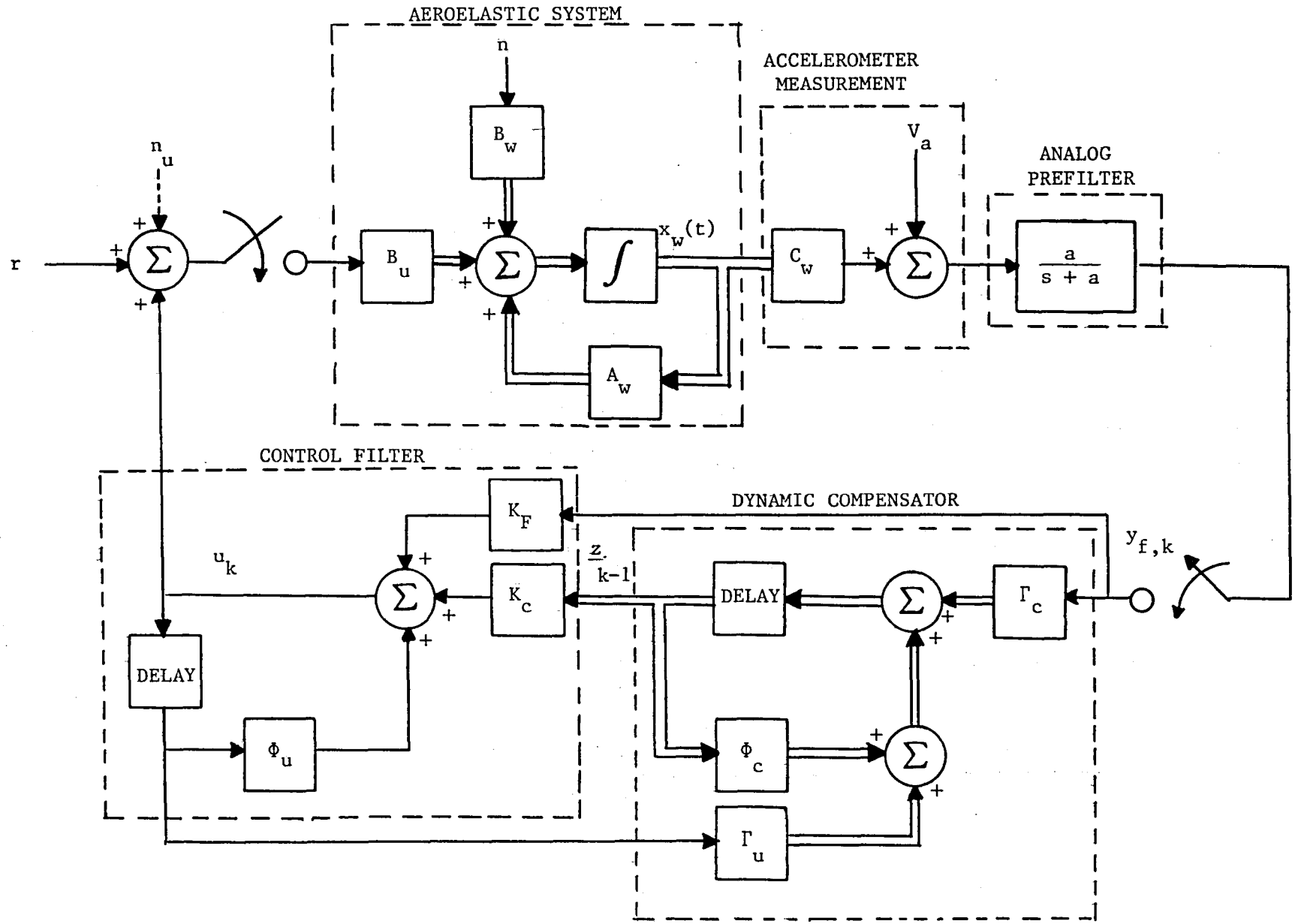

FIGURE 6 BLOCK DIAGRAM OF ALTERNATE CONTROL STRUCTURE

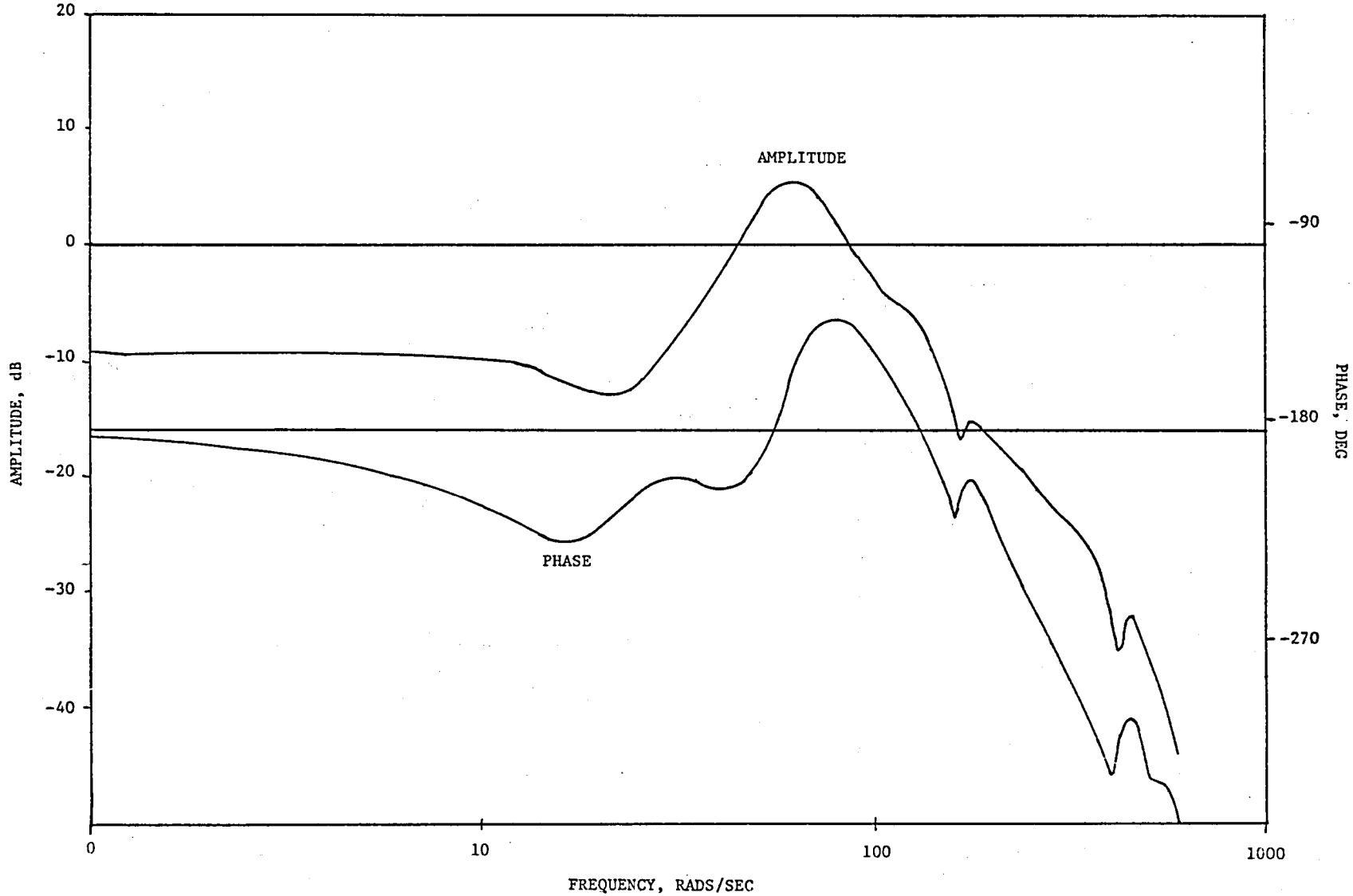

FIGURE 7 BODE PLOT OF ALTERNATE STRUCTURE CONTROL LAW USING X_u = 0.01 AT A DYNAMIC PRESSURE OF 8.0 kPa

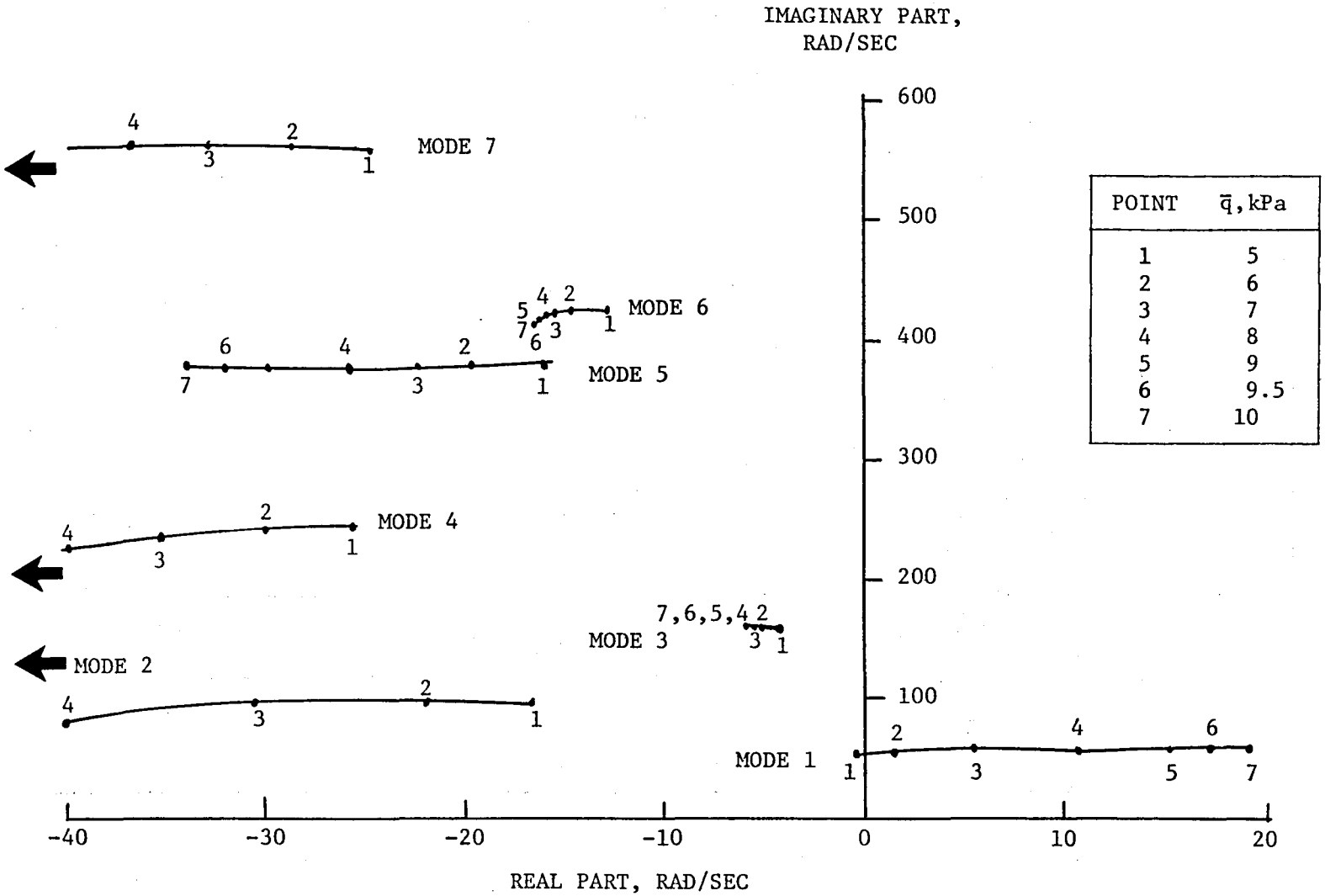

FIGURE 8 OPEN-LOOP DYNAMIC PRESSURE ROOT LOCUS AT MACH 0.9

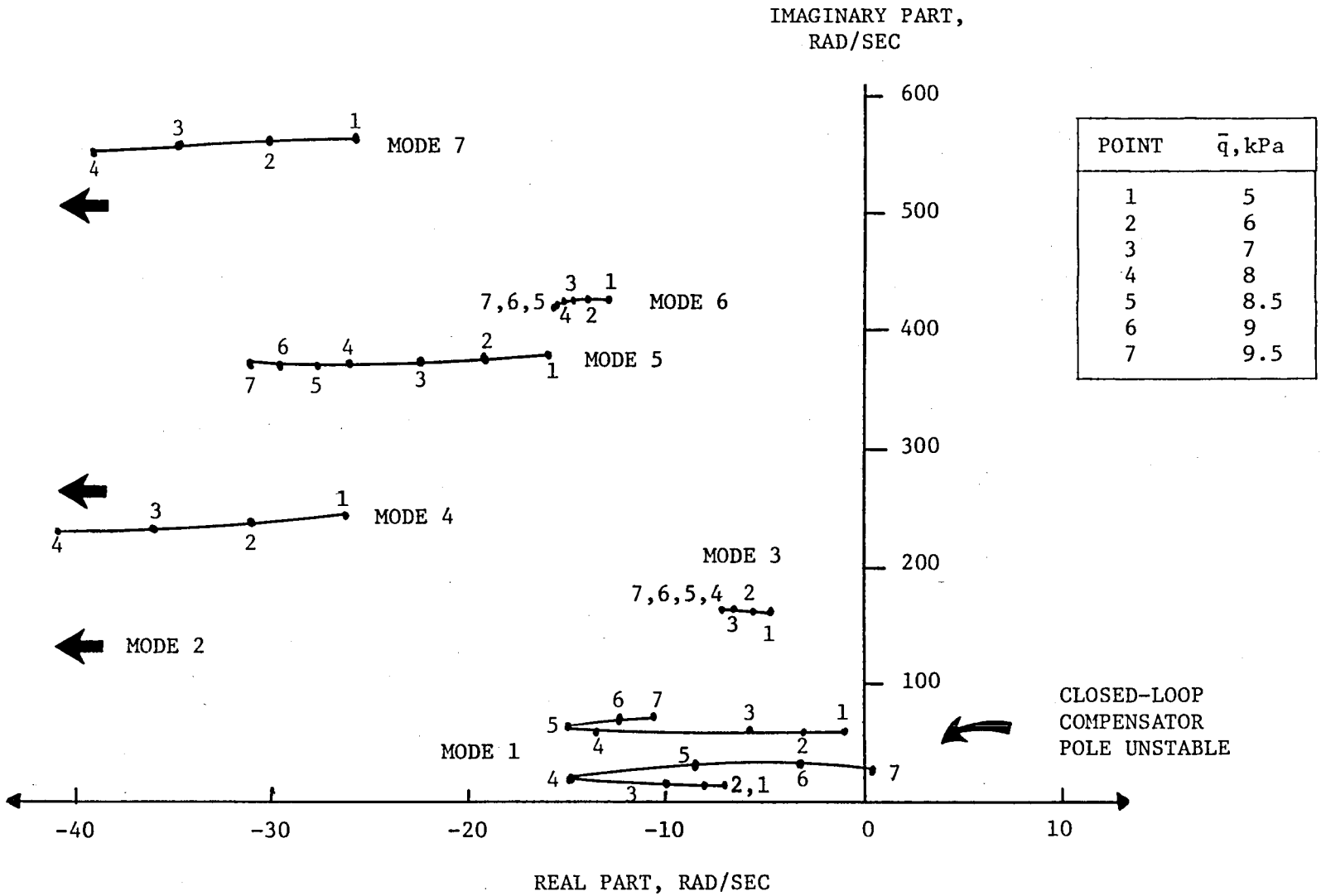

FIGURE 9 CLOSED-LOOP DYNAMIC PRESSURE ROOT LOCUS FOR CONSTANT GAIN DESIGN AT $\bar{q}$ = 8.0 kPas

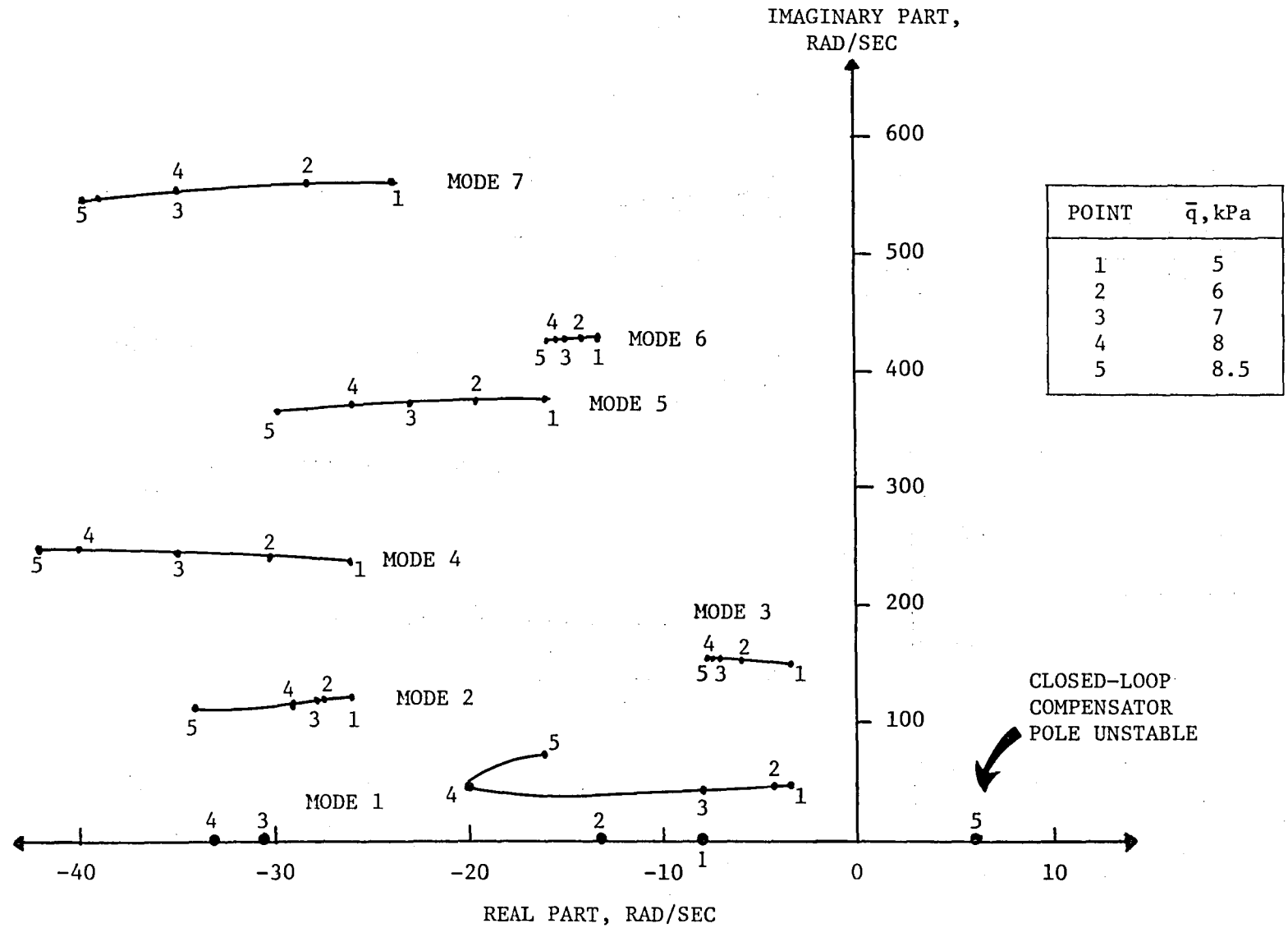

FIGURE 10 CLOSED-LOOP DYNAMIC PRESSURE ROOT LOCUS FOR SCHEDULED GAIN DESIGN

1. Report No.	2. Government Accession No.	3. Recipient's Catalog No.
NASA CR-165939		

4. Title and Subtitle	5. Report Date
ACTIVE FLUTTER SUPPRESSION USING OPTIMAL OUTPUT FEEDBACK DIGITAL CONTROLLERS	May 1982
	6. Performing Organization Code

7. Author(s)	8. Performing Organization Report No.
JOHN R. BROUSSARD AND NESIM HALYO	
	10. Work Unit No.

9. Performing Organization Name and Address	11. Contract or Grant No.
INFORMATION & CONTROL SYSTEMS, INCORPORATED 28 RESEARCH DRIVE HAMPTON, VA 23666	NAS1-16772
	13. Type of Report and Period Covered
12. Sponsoring Agency Name and Address	Contractor Report
NATIONAL AERONAUTICS AND SPACE ADMINISTRATION LANGLEY RESEARCH CENTER HAMPTON, VA 23665	14. Sponsoring Agency Code

15. Supplementary Notes

NASA LANGLEY TECHNICAL MONITOR: AARON J. OSTROFF

16. Abstract

A method for synthesizing digital active flutter suppression controllers using the concept of optimal output feedback is presented. A recently developed convergent algorithm is employed to determine constrained control law parameters that minimize an infinite-time discrete quadratic performance index. Low-order compensator dynamics are included in the control law and the compensator parameters are computed along with the output feedback gain as part of the optimization process. An input noise adjustment procedure is used to improve the stability margins of the digital active flutter controller. Results from investigations into sample rate variation, prefilter pole variation, control structure variation and gain scheduling are discussed. The study indicates that a digital control law which accommodates computation delay can stabilize the wing with reasonable rms performance and adequate stability margins.

17. Key Words (Suggested by Author(s))	18. Distribution Statement
ACTIVE CONTROL FLUTTER SUPPRESSION OPTIMAL CONTROL-APPLICATION OUTPUT FEEDBACK	UNCLASSIFIED - UNLIMITED

19. Security Classif. (of this report)	20. Security Classif. (of this page)	21. No. of Pages	22. Price
UNCLASSIFIED	UNCLASSIFIED	72	

For sale by the National Technical Information Service, Springfield, Virginia 22161

End of Document